Gas–Solid Two-Phase Flow in FCC Riser

Yiping Fan, Sheng Ye, Zhongxi Chao, Chunxi Lu, Guogang Sun, and Mingxian Shi
Dept. of Chemical Engineering, University of Petroleum, Beijing, 102200, P. R. China

FCC riser performance was examined in a large cold-riser model made of 0.186-m-ID plexiglass. In the prelift zone, distributions of particle velocity and local density in six cross sections were investigated, and the experimental results indicated that the whole prelift zone can be divided into three subzones in the axial direction. In the feedstock injection zone, some new flow parameters were introduced and five flow parameters in five different cross sections were measured. When a nozzle jet was injected, secondary flow of the jet exited in the vicinity of the riser wall due to vortices, and this flow moved forth at first and then merged into the main stream. Based on the gas–solid two-phase flow characteristics in each zone, the whole feedstock injection zone of the riser can be divided into four subzones. A new axial particle backmixing model and a simplified method for computing the radial distribution of the nozzle jet concentration in a different riser cross section can predict flow parameters of particles and the jet.

Introduction

The riser reactor is one of the most important units in the fluid catalytic cracking process, which is widely used in the modern petroleum refinery industry. A riser reactor can be divided into four parts from bottom to top according to their functions: the prelift zone, the feedstock injection zone, the full-reaction zone, and the quenching zone.

In the prelift zone, catalysts enter the riser reactor from the regenerator and are then conveyed by the prelift gas. When the gas–solid two-phase mixture reaches the feedstock injection zone, catalysts will mix with the feed oil injected through feedstock nozzles and begin to react rapidly. The distributions of the particle concentration and of the particle velocity form in the prelift zone and the distributions will greatly influence the contact efficiency of catalysts and feedstock oil. Moreover, determining the best proper feedstock injection position also depends greatly on the catalyst flow conditions, such as its concentration and velocity in this zone. Therefore, a detailed investigation of the flow pattern in the prelift zone is of significance for the design and operation of an FCC riser.

In the feedstock injection zone, feed oil is introduced into the riser through the feed nozzles, and the heavy oil comes in contact with the high-temperature catalysts and then reacts rapidly. The contact and flow conditions of these two phases will directly affect the FCC unit. It is obvious that knowledge of the dynamics of feed jet and solids motion in this area is of considerable significance for improving reactor operation and design.

Correspondence concerning this article should be addressed to Y. Fan.

Previous Work

Previous researches indicate that gas–solid two-phase flow in a riser can be described as a bottom dense area and an upper dilute area. The upper dilute area, including the radial annular-core flow structure and the cluster nature of dilute gas–solid suspensions, has been extensively studied in past decades. For the prelift zone, however, only very limited information is available in the literature. The prelift zone is either described as a turbulent bed, as by Brereton and Grace (1993), or as a bubbling bed, as by Svensson (1996). Miller and Gidaspow (1992) observed an asymmetric flow pattern in the radial profiles of solids flux and velocity in the bottom region of a riser, but a detailed description of the flow characteristics in the prelift zone remains very deficient.

The flow in the feedstock injection zone is very complex, perhaps the most complex flow in a reactor. It can be described as "multiple confined jets injecting into a three-dimensional, three-phase flow." The literature contained little of the dynamic behavior of the gas and solid phases in this zone, and still much less of the feed jet diffusion.

There are only a few *related* articles about three aspects.

Jet in crossflow

Examples of this type of research can be found mainly in pieces on the transition flight of the V/STOL aircraft. Keffer and Baines (1963), Moussa and Sykes (1977), Crabb and Whitelaw (1981), Andreopoulos and Rodi (1984), and Subramaniam (1999), among others, have done quite a bit of work in this field. They applied hot-wire, triple-wire, and X-wire measurements to flow visualization techniques to investigate the velocity and vortices distribution in the mixing regime, respectively. Needham et al. (1988) and Sergio et al. (1989) even used a very practical asymptotic method to predict the velocity distribution in the mixing regime. But velocity and vortices were the key investigated objectives of their work, not mixing and contact between jet and crossflow, which are emphasized in the riser–nozzle system. Furthermore, the velocity ratios in their experiments or computations were too small (usually less than 3) compared with the riser–feed nozzle system. Moreover, the occurrence of the dense region makes the asymptotic method almost inapplicable in the research of the FCC riser feedstock injection zone.

Secondary air injection into a fluidized bed

Secondary air injection into the fluidized bed is widely used in CFB coal combustors. It is somewhat similar to the riser–feed nozzle system. In this field, Lummi and Baskakov (1967) injected a CO_2 tracer with an air jet and measured subsequent CO_2 concentration in the bed to obtain mixing rates. Zenz (1968) presented a curve to predict horizontal jet penetration depth. Shakhova and Minayev (1968) derived an expression for horizontal jet penetration depth. Referring to a specific design of a cap-type air distributor, Kozin and Basakov (1967) proposed a penetration correlation. Merry (1971) measured the penetration depth of a horizontal air jet injected into fluidized beds of sand, kale seed, and steel shot, and derived a simple model for jet penetration depth prediction. The dynamics of a jet discharged into a fluidized bed were reported by Shakhova and Minakev (1968), using the ratio of the length of the gas plume to the height of the fluidized bed above the nozzle to describe two characteristic modes of jet behavior, bubble flow, and coherent flow. Two recent papers by Xuerub et al. (1991a,b) describe the behaviors of thin, two-dimensional, horizontal and inclined jets. In these papers, several important jet characteristics were presented, including the proclivity of bubble tracks to hug the wall through which the jet is introduced. In addition, the existence of a particle dragging zone is discussed. Chen and Weinstein (1993) used X-ray measurement to obtain profiles of the mean solid fraction and fluctuation in a horizontal nozzle–rectangular bed system, and the autocorrelation analysis indicated that there are three discernible regions in the jet-influenced area. Agillion et al. (1996), Arena et al. (1993), and Yong et al. (1993) investigated the solid-phase flow behavior, such as the axial distribution of the solid fraction, and the radial distribution of the solid-mass flux when secondary air was injected into the CFB. Their researches were mainly concerned with the influence of injection height, jet angle, and velocity ratio on the flow behavior of CFB.

In CFB coal combustors, burning particles more efficiently is the final aim, and thus the most desirable condition is the occurrence of a steady reflux regime. In the riser feedstock injection zone, however, reflux or backmixing is disadvantageous to the FCC unit. Moreover, the operating conditions, such as the velocity ratios and the scales of the experimental devices in CFB coal combustors, are also much different from the FCC riser. In addition, higher mixing efficiency of feed jet and catalyst particles is the most crucial factor to cracking reactions in the FCC riser. The concentration and velocity distribution of feed oil and of particles in the riser are of greater importance than other factors considered, such as the penetration depth, the flux rate, and the hydrodynamic behavior of CFB.

Simulation

Simulation is one of the most significant means by which a comprehensive understanding of the gas–solid two-phase flow in the feedstock injection zone of the FCC riser can be obtained. The works of Thelogs et al. (1996) and Gao (1997) are quite representative. They incorporated a detailed ten-lump kinetic model into 3-D computational fluid dynamics techniques. Even the simulation of feedstock vaporization inside the riser was addressed in detail. In addition, Albrech et al. (2001) performed an unsteady simulation of three-phase gas-droplet-particles turbulent flow with heat and mass transfer in the feedstock injection zone of an industrial FCC riser using a two-fluid modeling approach. The relevant configurations for further investigation with LES simulation, combined with deterministic Lagrangian tracking, are defined.

The numerical simulation, however, is too complex for engineering purposes. Moreover, some boundary conditions and initial conditions in the simulation cannot be precisely given. They have to be determined by experiment.

Based on the preceding discussion, it is obvious that experimental research on the flow pattern in the prelift zone, especially in the feedstock injection zone of the FCC riser, is quite limited.

This article first depicts the flow-pattern feature in the prelift zone, and then describes the mixing and contact between the nozzle jet and catalysts, features of the gas-solid two–phase and it covers the flow in the feedstock injection zone.

Experimental Studies

Experimental equipment

The experimental setup used is shown in Figure 1. It is mainly composed of a riser, a gas–solid separation system, and a recirculation system. The riser consists of a series of 186-mm ID flanged plexiglass pipes with a height of 14 m. At a height of 4.5 m above the gas distributor, four nozzles corresponding to the feedstock nozzles are installed with an angle of 30° to the riser axis, the same as in most industrial devices. The gas–solid separation system consists of a disengagement chamber located at the end of the riser, a cyclone, and a bag filter. The solid recirculation system comprises a 300-mm ID plexiglass downcomer fitted with a butterfly valve for solid flux measurement. The solid flux is calculated by measuring the time for a known volume of solids accumulating on top of the butterfly valve after the valve is closed. Both

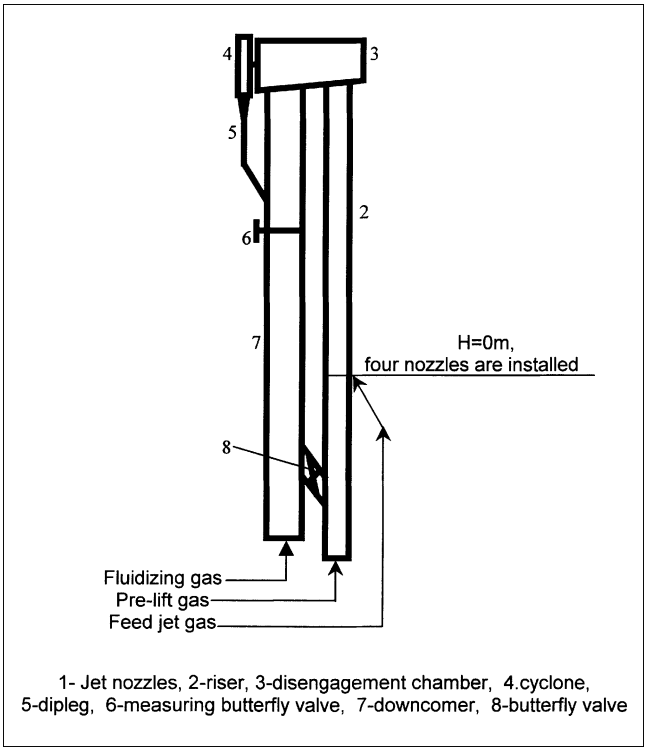

Figure 1. Experimental apparatus.

the prelift gas and nozzle jet gas are air, supplied by Roots blowers, and their flow rates are controlled by different rotameters. The solids were typical FCC catalysts. Their properties are given in Table 1. The operating conditions are shown in Table 2

Measurement and data analysis

In this paper, the local density and the local axial particle velocity in different positions inside the riser are measured with fiber optic probes.

Measurement of Local Density. As we all know, when a beam of light irradiates a cluster of particles, part of the light will be reflected while the other part will be absorbed. The principle of optical-fiber measurement is based on the fact that the intensity of reflected light depends on the density of the particle cluster irradiated.

The measuring system must be calibrated before each measurement. In a box shielded from natural light, the reflected light intensity, c_0, in the absence of particles, and the intensity, c_b, corresponding to bulk density of particles, are measured, respectively. Then the local density in the riser can be determined by the linear interpolation $\rho = \rho_b(c - c_0)/(c_b - c_0)$, where c denotes the reflected light intensity obtained at the measured position in the riser.

Measurement of Particle Axial Velocity. It is well known that the velocity of an object can be determined by the displacement value divided by its shift time. In a complex gas–solid two-phase flow field, since the particle velocity can be measured exactly only if the distance of the two transducers is close to the diameter of the measured particles, the fiber will be an effective measuring method. In this measurement, five optical-fiber probes arranged in a line were placed in a stainless-steel tube, two receiving incident light and the other three receiving reflected light. They were transformed to three electrical signals A, B, and C by a photomultiplier tube. Therefore, three electrical signals T_a, T_b, and T_c can be obtained when a particle passes through the optical-fiber probes. The shift times are $\Delta T_a = T_c - T_a$ and $\Delta T_b = T_b - T_c$, respectively. The sequence of these signals is $T_a \rightarrow T_c \rightarrow T_b$ or $T_b \rightarrow T_c \rightarrow T_a$. It is determined by the direction of particle flow so that we can obtain the statistical result of particle numbers and of mean velocities that flow upward and downward. In this measurement, signal C is introduced between probe A and probe B for the sake of judging correlation. Moreover a logic circuit is used to judge whether the shift time, ΔT_a, is equal to ΔT_b, considering that any particle flow through a span of not less than 1 mm can be treated as traveling at a certain speed. Any signal that reflects ΔT_a not equivalent to ΔT_b should be neglected, thus allowing any false correlation signal to be eliminated.

Table 1. Properties for Tested FCC Catalyst

Particle density (kg/m^3)	1,310
Bulk density (kg/m^3)	843
Mean particle size (μm)	65
Particle size range (μm)	30 ~ 90

Table 2. Operative Condition

Prelift gas superficial velocity (m/s)	2.25 ~ 5.1
Nozzle jet velocity (m/s)	41.7 ~ 83.3
Solid mass flux in riser (kg/m^2·s)	45 ~ 213

Measurement of Jet Flow Characteristic in a Riser. A hydrogen tracer technique is applied to investigate the diffusion and flow characteristics of jet gas after it is injected into the riser. Hydrogen is injected into the four nozzles in pulses entering the riser together with nozzle jet. Ten sampling probes were placed in five different riser cross-sections in a proper order, and every sampling probe is placed in a different radial position in each section. Analysis of the concentration and residency time distribution of the hydrogen tracer in different positions reveals roughly the diffusion and flow patterns of the nozzle jets.

Particle backmixing ratio α

The local particle velocity measured by the optic-fiber probes indicated that particles inside the riser move upward and downward dynamically wherever the radial location is. Even in the upper part of the riser, the downflow of the particles can be detected in the central region. Because the proportion and magnitude of the upflowing particles are quite different from those of the downflowing particles, the time-averaged particle velocities are diverse at different locations. In fact, the solid phase in a riser is not a continuous phase from an Euler point of view. Therefore a new parameter α, called the *particle backmixing ratio*, is introduced and is defined as the value of $(n_d \times v_d)/(n_u \times v_u)$ in a certain location during a given sampling time. The particle backmixing ratio reflects the momentum ratio of the particles whose velocities

are downward to those of the upward particles. The parameters n_d, v_d, n_u, v_u can be obtained directly by an optical-fiber probe.

It is obvious that the mean axial velocity of particles in a given measuring position can be expressed by

$$v = \frac{n_u v_u - n_d v_d}{n_u + n_d}.$$

Eigenconcentration of the jet $\overline{C}$

In this research, the hydrogen tracer injection into the nozzles is pulsatile; in other words, the injecting time is very transient (usually 30 ms) and the flux of the tracer is much less than that of the prelift gas and nozzle jets at each location. Therefore a new parameter must be introduced to diminish the error caused by the measurement system and the intense turbulence, and especially to decrease the error caused by the different tracer injection volume at different operating conditions. The definition of the eigenconcentration of the jet is expressed as

$$\overline{C} = \lambda \frac{C_i}{\sum C_i} \left(\frac{Q_j}{Q_j + Q_r} \right)$$

in a given position, where the term $Q_j/(Q_j + Q_r)$ is introduced to avoid the error that results from the difference between the continuous feedstock and the pulsatile injection of the tracer. It is as though the Q_j volume of the solute is dissolved in the $Q_j + Q_r$ solution volume. The sampled tracer concentration, C_i, can be obtained directly by the sampling system. Here λ is the density coefficient and is designated 1 for processing convenience.

The parameter $\overline{C}$ can reflect the relative concentration of the jet gas in different riser locations after it is injected into the riser.

Eigenvelocity of the jet u_e

The definition of this parameter is $u_e = k/t$. The eigenvelocity of the jet reflects the relative velocity of jet gas in a different riser position. The parameter t denotes the mean residence time of the hydrogen tracer in the sampling position, which can be obtained directly using the sampling system, while the number k is a constant.

Flow Characteristics in the Prelift Zone. The evolutions of the typical radial distributions of the time-averaged local density and of the particle axial velocity along the height of the riser are presented in Figures 2 and 3. The data were taken at an operation of solid mass flux of 113 kg/m^{2}s and superficial prelift gas velocity of 4.3 m/s, while the nozzle jet velocity was 0 m/s. The dimensionless radial coordinate of -1 is close to the downcomer.

Some obvious characteristics of the local density in the riser are shown in Figure 2. First, the local density decreases with an increase in the axial height. Second, the flow pattern in the upper part of the riser can be regarded as a typical core-annular flow, whereas there are some distortions in the bottom region. The radial density profile in the bottommost region is quite asymmetric due to the effects of the bottom particles and gas inlet, while numerous symmetric and flatter profiles are observed in the upper part of the riser.

In the cross sections at 0.9 m, 1.5 m, and 2.5 m above the gas distributor, the time-averaged local density just above the solid inlet is higher than that on the opposite side, which can be seen clearly in Figure 2. The asymmetry of the bottom radial density profiles disappears around of 2.5 m to 4.5 m above the gas distributor. The radial density distribution gradually becomes a flat symmetric profile in the upper region above 4.5 m and a typical core-annular structure is obtained. The height at which the asymmetric radial profile becomes a symmetric profile is important for the design of the FCC riser feedstock injection zone and for the installation of feedstock nozzles, since the asymmetric and nonuniform density profile is generally believed to be disadvantageous in an FCC unit.

The measured particle velocities generally increase with the riser's height, which demonstrates significant solid acceleration in the prelift zone along the riser, as shown in Figure 3.

At the lower heights of 0.9 m, 1.5 m, and 2.5 m above the gas distributor, the radial particle velocity profiles exhibit a strong asymmetric quality, with the maximum velocity positions shifting to the opposite side to the particle inlet. Particles just above the solid inlet flow up much more slowly than those on the opposite side. This trend prevails up to a height of approximately 4.5 m.

As can be seen from the preceding discussion, the whole prelift zone can be divided into three axial subzones. In this article, they are called the mixing accelerating subzone (between 0 and 4.5 m), the uniform accelerating subzone (between 4.5 and 6.5 m), and the fully developed subzone (above

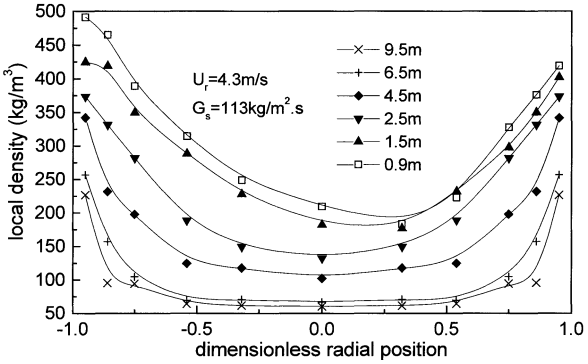

Figure 2. Radial distribution of local density for various riser heights in prelift zone.

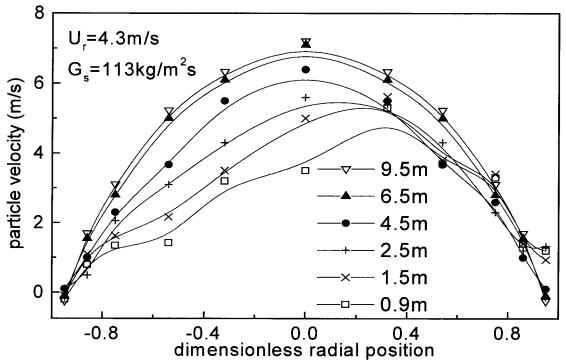

Figure 3. Radial distribution of particle velocity for various riser heights in prelift zone.

6.5 m). In each zone, the flow characteristic is much different from the others, including the mathematical description.

The diffusibility equation and the continuity equation for the solid phase are given as follows:

$$\upsilon_r \partial\rho/\partial r + \upsilon_\theta \partial\rho/r\partial\theta + \upsilon_z \partial\rho/\partial z = D_j\left[\partial\left(r\partial\rho/\partial r\right)/r\partial r + \partial^2\rho/r^2\partial\theta^2 + \partial^2\rho/\partial z^2\right] \quad (1)$$

$$\frac{\rho\upsilon_r}{r} + \upsilon_r\frac{\partial\rho}{\partial r} + \rho\frac{\partial\upsilon_r}{\partial r} + \rho\frac{\partial\upsilon_z}{\partial z} + \upsilon_z\frac{\partial\rho}{\partial z} + \upsilon_\theta\frac{\partial\rho}{r\partial\theta} + \rho\frac{\partial\upsilon_\theta}{r\partial\theta} = 0. \quad (2)$$

Here the parameter $\rho = \rho_p\epsilon_p$.

In the mixing accelerating subzone, particles are being accelerated, while all flow parameters are distributed asymmetrically, which is denoted as $\partial/\partial\theta \neq 0$, $\partial/\partial z \neq 0$, and $\partial\upsilon_z/\partial r \neq 0$. After analyzing Eqs. 1 and 2 simultaneously, we see that the mixing accelerating subzone can be described as a typical three-dimensional flow field.

In the uniform accelerating subzone, asymmetrical distribution has already disappeared, but particles are still accelerating. By analyzing Eqs. 1 and 2 simultaneously and considering $\partial/\partial\theta = 0$, $\partial\upsilon_z/\partial z \neq 0$ of the flow parameter distribution, we see that $\upsilon_z \neq 0$, $\upsilon_r \neq 0$ indicate that the uniform accelerating subzone is a representative two-dimensional flow area in which the mass exchange of particles occurs intensely between the dense phase region near the wall and the central dilute phase region.

In the fully developed subzone, the two-phase flow has already developed into a typical annular-core structure by the time the particles have finished accelerating. If we analyze Eqs. 1 and 2 simultaneously, and considering $\partial\rho/\partial z = 0$, $\partial/\partial\theta = 0$, and $\partial\upsilon_z/\partial z = 0$ of the flow parameters distribution, we see $\upsilon_z \neq 0$ shows that this zone can be characterized as a typical one-dimensional flow region.

From the preceding analysis, we can draw two important conclusions about how to decide the proper feedstock nozzle position.

First, the nozzles should not be placed in the mixing accelerating subzone due to its asymmetric distributions of flow parameters, which is believed to be disadvantageous to the FCC unit. That is to say, the nozzle should be fixed at a height of $H_j \geq 4.5$ m.

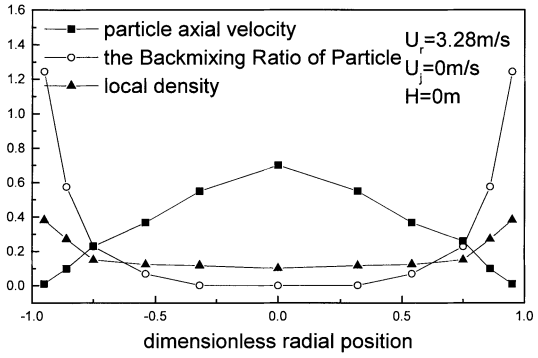

Figure 4. Measured parameters at the nozzles' installed height when there is no jet injection.

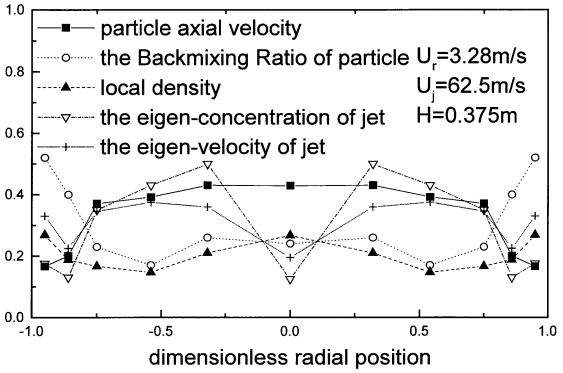

Figure 5. Measured parameters at 0.375 m above the nozzles.

Second, the fully developed subzone is not the most appropriate position to install feedstock nozzles either, though local concentration and particle velocity are symmetrically distributed. Instead, it is because of its much lower mean-density value in this area. Furthermore, the larger density and particle velocity distribution gradients near the wall region, especially, in the area of $\tilde{r} > 0.86$, are larger than those in the uniform accelerating zone, and that makes it unsuitable for nozzle fixing.

The most proper installation location of feedstock nozzles is in the uniform accelerating subzone, that is, the appropriate location for installing feedstock nozzles is $H_a \geq H_j \geq 4.5$ m, which can be advantageous to the contact and mixing of catalysts and feed oil.

Based on the experimental data, we can obtain the particle acceleration length and axial mean voidage distribution correlation:

$$\frac{H_a}{d_p} = 9.14\times10^4\left(Re_g\right)^{0.034}\left(Re_p\right)^{0.168}\left(\frac{D}{d_p}\right)^{0.08} \times\left(\frac{\rho_p-\rho_g}{\rho_g}\right)^{0.493}(Ar)^{-0.535}(Fr)^{-0.41} \quad (3)$$

$$\bar{\epsilon} = 0.3296\left(Re_p\right)^{-0.1145}\left(\frac{D}{d_p}\right)^{-0.1119}\left(\frac{\rho_p-\rho_g}{\rho_g}\right)^{-0.0784} \times(Fr)^{0.1249}\left(\frac{z}{d_p}\right)^{0.0686}. \quad (4)$$

The applicability of Eqs. 3 and 4 is subject to the following constraints:

Re_g = ranging from 27,560 to 62,600;
Re_p = ranging from 122 to 693;
Fr = ranging from 8,756 to 45,161.

Flow Characteristics in Feedstock Injection Zone. In this article, four nozzles corresponding to feedstock nozzles are installed at a height of 4.5 m above the gas distribution.

We plot all the measured flow parameters in one diagram so that we can determine their various relationships, which are shown in Figures 4–8. It is an effective way to analyze the

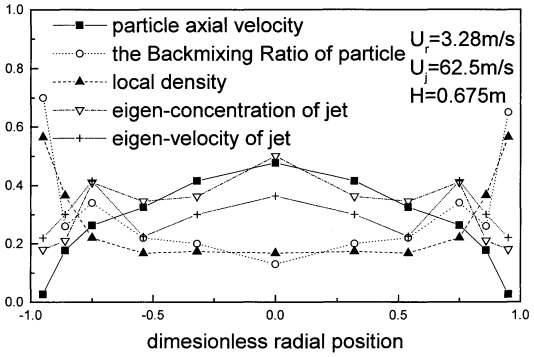

Figure 6. Measured parameters at 0.675 m above the nozzles.

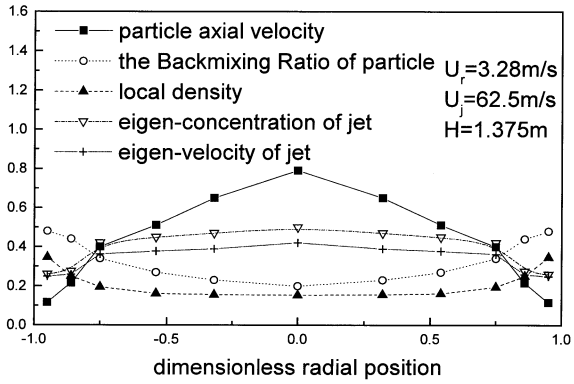

Figure 8. Measured parameters at 1.375 m above the nozzles.

mixing process and flow characteristics in the feedstock injection zone, although the units or dimensions of these parameters are quite different. In these five figures, a typical operating condition is taken at which the nozzle jet velocity is 62.5 m/s, the prelift gas velocity is 3.28 m/s, and the solid flux is 113 kg/m^2·s.

In these figures, the unit of particle velocity is 10 m/s, while the local density is 1,000 kg/m^3.

H = 0 m, U_r = 3.28 m/s, U_j = 0 m/s. Figure 4 shows when there was no jet injecting, the relationship of the particle backmixing ratio, the particle velocity, and the local density in the riser cross section, where the nozzles were installed ($H = 4.5$ m). As discussed earlier, the gas–solid two-phase flow in this figure presents a typical annular-core structure (referring to Figures 2 and 3). Another important characteristic is that the inflexion of the particle backmixing ratio profile exactly matches that of the local density distribution, which demonstrates that the particle concentration is the dominant factor to its backmixing when there is no jet injection.

H = 0.375 m, U_r = 3.28 m/s, U_j = 62.5 m/s. Figure 5 shows the relationships of the particle backmixing ratio, the particle velocity, the local density, the eigenconcentration of the jet, and the eigenvelocity of the jet in the cross section at 0.375 m above the nozzles.

A: Features of the Jet. Under the free-jet condition, the jet should reach the central line at a height of 0.161 m above the nozzles. But under this operating condition, a minimum of the jet eigenconcentration appears at the center of the cross section, which denotes that the jet has not yet reached the central line of the riser because of intense underwashing by the flow taking place in the prelift zone. At the same time, the end of the jet appears at $\tilde{r} = 0.32$ as the maximum of jet eigenconcentration in this cross-section coming from there, and the deflexion angle of the jet even comes to 20° compared with that of the free jet. In the vicinity of the riser wall, the rise in the jet eigenconcentration and in the jet eigenvelocity means a jet of secondary flow arises there relative to the jet mainstream. The boundary between the mainstream and the secondary flow of the jet is located at $\tilde{r} = 0.86$.

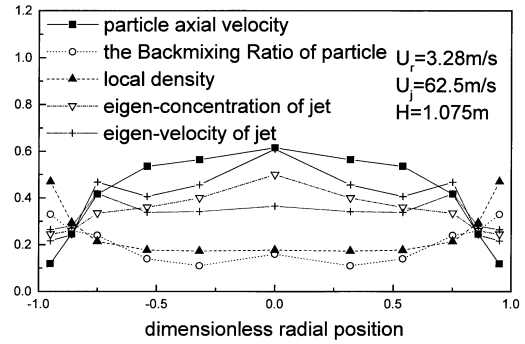

Figure 7. Measured parameters at 1.075 m above the nozzles.

B: Features of the Solid Phase. At least two noticeable features of solid phase are observable. First, the flow feature is very different from the typical annular-core structure due to jets injection. The whole cross section can be divided into three regions: the wall dense-phase region ($\tilde{r} \geq 0.86$), the annular transition region ($0.54 \leq \tilde{r} \leq 0.86$), and the central hypodense-phase region. ($0 \leq \tilde{r} \leq 0.54$). The highest density appears in the wall dense phase region, while the lowest density is in the annular transition region. In the wall dense-phase region, the value of local density increases with radial location, but in the central hypodense-phase region, the trend is exactly the opposite. With regard to the annular transition region, the local density remains almost a constant in the radial direction.

Second, in the wall dense-phase region and the central hypodense-phase region, local density is very important to the value of particle backmixing, which denotes that the particle backmixing is more intense in a higher-density region. The backmixing ratio increases with the local density value. On the other hand, jet eigenmomentum plays a dominant role in determining the particle backmixing ratio in the annular transition region. The influence of jets can be seen clearly in this cross section.

The particle velocity radial distribution is also much different from that of the annular-core structure; the velocity maximum is not located at the riser axis but shifts to $\tilde{r} = 0.32$. The influence of the jets is apparent.

In this cross section, another distinct characteristic is that the boundary between the mainstream and secondary flow of the jet coincides exactly with that of the wall dense-phase

region and the annular transition region, while the boundary of the annular transition region and central hypodense phase region is located in $\tilde{r} = 0.54$, at which the $\partial v/\partial r$ change sign.

Since the jet mainsteam greatly affects the flow characteristic, especially on the local density distribution at this height, this cross section can be called the jet mainstream influence subzone.

In the axial direction, this subzone ends at the height where the jet mainstream reaches the riser axis, where $d\overline{C}/d\tilde{r}$ is equal to 0.

$H = 0.675$ m, $U_r = 3.28$ m/s, $U_j = 62.5$ m/s. Figure 6 shows the radial distribution of the five parameters in the cross section at 0.675 m above the nozzles.

A: Feature of the Jet. In this cross section, a minimum of the jet eigenconcentration and jet eigenvelocity occurs at $\tilde{r} = 0.54$, while the maximal value of these two parameters in this cross section occurs at the $\tilde{r} = 0$ position. At the same time, the second local maximal value of the jet eigenconcentration and jet eigenvelocity occurs at $\tilde{r} = 0.75$. This showed that the jet mainstream had already reached the axis of the riser and the jet secondary flow had extended gradually in this cross section because the boundary between the jet mainstream region and the jet secondary flow region had shifted to the $\tilde{r} = 0.54$ position.

B: Feature of the Solid Phase. The whole cross section can be divided into two areas according to the two-phase flow characteristics: the wall dense-phase region ($\tilde{r} \geq 0.54$) and the central dilute-phase region ($0 \leq \tilde{r} \leq 0.54$), which resembles the typical annular-core structure to some extent. The local density value increases with the radial position, but in the wall dense-phase region, the local density assumes a higher value and a sharper gradient than those of a typical annular-core structure.

In the wall dense-phase region, the local density is the main factor in particle backmixing, which means that the particle backmixing becomes more intense in a higher density region, too. At the same time, jet eigenmomentum becomes a dominate factor in determining the particle backmixing ratio in the central dilute region.

Another very crucial characteristic of this cross section is that the maximum particle backmixing originates in these five tested cross sections, and in the wall dense-phase region in particular, the backmixing is very intense. This is because in this cross section, the flow of particles resembles "the flow round a blunt body." Many particles flow transversely in the radial direction. Moreover, the extension of the jet secondary flow also contributes particles flowing transversely, which results in the frequent collision of particles. Then violent backmixing takes place. In the industrial riser reactor, charring often occurs at a height of $0.6 \sim 1$ m above the atomizing nozzles. The prevalent viewpoint about it was "feedstock jet impinging on the opposite riser wall of the atomizing nozzle." But the main cause presented in this article might be that the flow of particles resembles "the flow round a blunt body" and the extension of the jet secondary flow. This opinion will be presented in detail in a future article.

The particle velocity distribution is close to that of the typical annular-core structure at this height. The maximal velocity is found at the riser center and the minimum velocity near the wall. But the radial velocity gradient is much greater than that of a typical annular-core structure.

In this cross section, another salient feature is the boundary between the mainstream region and the jet's secondary flow region, which corresponds exactly to that of the wall dense-phase region and the central dilute-phase region, just as in the jet mainstream influence zone.

This cross section can be defined as the jet secondary flow influence subzone based on the fact that the jet secondary flow plays a decisive role in jet diffusion and particle flow feature in this cross section.

In the axial direction, this subzone ends when the boundary of the dilute- and dense-phase regions appears at $\tilde{r} = 0.75$, which denotes that the regime has re-assumed the typical annular-core structure again.

$H = 1.075$ m and 1.375 m, $U_r = 4.3$ m/s, $U_j = 83.3$ m/s. Figures 7 and 8 show the profiles of those parameters in the cross sections at 1.075 m and 1.375 m above the nozzles.

A: Features of the Jet. In these two cross sections, the minimum of the jet eigenconcentration and the jet eigenvelocity appear at the riser wall, while the maximum of these two parameters occur in the $\tilde{r} = 0$ location. Moreover, the secondary jet flow disappeared.

B: Feature of the Solid Phase. The two-phase flow in these two cross sections behaves like a typical annular-core structure again. The whole cross section can be divided into two regions according to two-phase flow features: the wall dense-phase region ($\tilde{r} \geq 0.75$) and the central dilute-phase region ($0 \leq \tilde{r} \leq 0.75$). The local density value increases with the radial position. The local density is again a crucial factor to the particle backmixing, which means that the particle backmixing increases or decreases depending on the variation of the local density. This is consistent with the no jet injection condition.

The particle velocity distribution also shows the annular-core structure feature. The maximal velocity is located at the riser axis, while the minimum velocity is near the wall.

The concentration distributions of the jet and solid demonstrate that the flow field has resumed the typical annular-core structure. Moreover, in this section, almost all inflexions of the flow parameters arise in the same position (at about $\tilde{r} = 0.75$). This shows that mixing between the nozzle jets and the solid phase coming from the prelift zone has been completed.

These two cross sections can be defined as the mixed-developing subzone, according to the flow characteristics.

$H = -0.2$ m, $U_r = 4.3$ m/s, $U_j = 83.3$ m/s. Figure 9 shows the particle backmixing ratio, the particle velocity, and the local density in the section 0.2 m below the nozzle.

The hydrogen tracer was not detected in this cross section. This demonstrates that there is no large-scale backmixing of feedstock jet upstream of the nozzles.

In this section, the two-phase flow is different from the typical annular-core structure due to the effect of the jet injection, although the nozzle jets did not reach this section directly. The whole cross section can be divided into three regions: the wall dense-phase region ($\tilde{r} \geq 0.86$), the density reforming region ($0.54 \leq \tilde{r} \leq 0.86$), and the central dilute-phase region. Their positions correspond exactly to the three regions in the mainstream jet influence zone. The highest density value appears in the wall dense-phase region, while the lowest density occurs in the central dilute-phase region. In the wall dense-phase region and the central dilute-phase region, the value of the local density increases with the radial

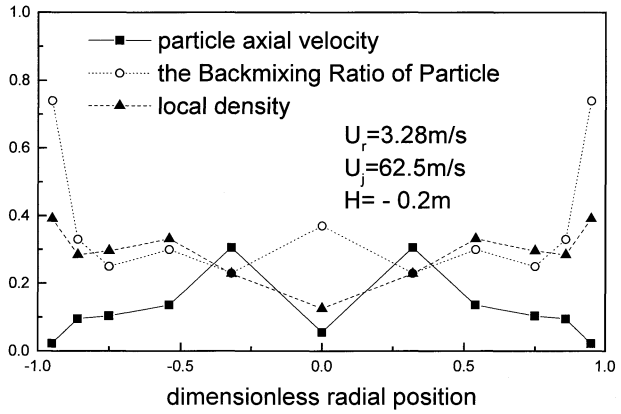

Figure 9. Measured parameters at 0.2 m below the nozzles.

position, but in the density reforming region, the trend is exactly the opposite.

Moreover, the particle velocity distribution is also much different from the typical annular-core structure. The profile of the velocity distribution assumes approximately an M shape. The maximum velocity is at the position $\tilde{r} = 0.32$, which corresponds nicely to the positions of the jet mainstream in the jet mainstream influence zone. This means the entraining of jets is very intense.

The particle backmixing distribution profile becomes approximately W shaped. Two maximum values of the particle backmixing ratio occur at $\tilde{r} = 0$ and $\tilde{r} = 0.54$, except in the region near the wall, which agrees exactly with the velocity distribution.

This cross section can be defined as the upstream influence subzone according to the flow feature.

Flow structure in the feedstock injection zone of a riser

It is obvious in the feedstock injection zone of the riser that two-phase flow differs from the typical annular-core structure after the jet injection. The feedstock injection zone can be divided into four subzones based on the flow behavior of jet and the solid phase. Each zone can also be divided into two or three regions in the radial direction. The flow structure in the feedstock injection zone is shown in Figure 10.

Analysis of the mixing process

As discussed earlier, the mixing process of the nozzle jet and the two-phase flow coming from the prelift zone can be obtained. Figure 11 shows the mixing process in the feedstock injection zone.

In Figure 11, the black arrow represents a catalyst particle, the gray arrow denotes prelift gas, while the white arrow indicates the feedstock jet. When the nozzle jet is injected into the riser, the two-phase flow coming from the prelift zone is separated into two parts, first by the different relaxation time between gas and gas and gas and solid. The prelift gas is entrained toward the nozzle exit, while the particles are "blown" toward the riser center. At the same time, the nozzle jet is also separated into two parts: the mainstream and the secondary flow. With the jet secondary flow entraining cir-

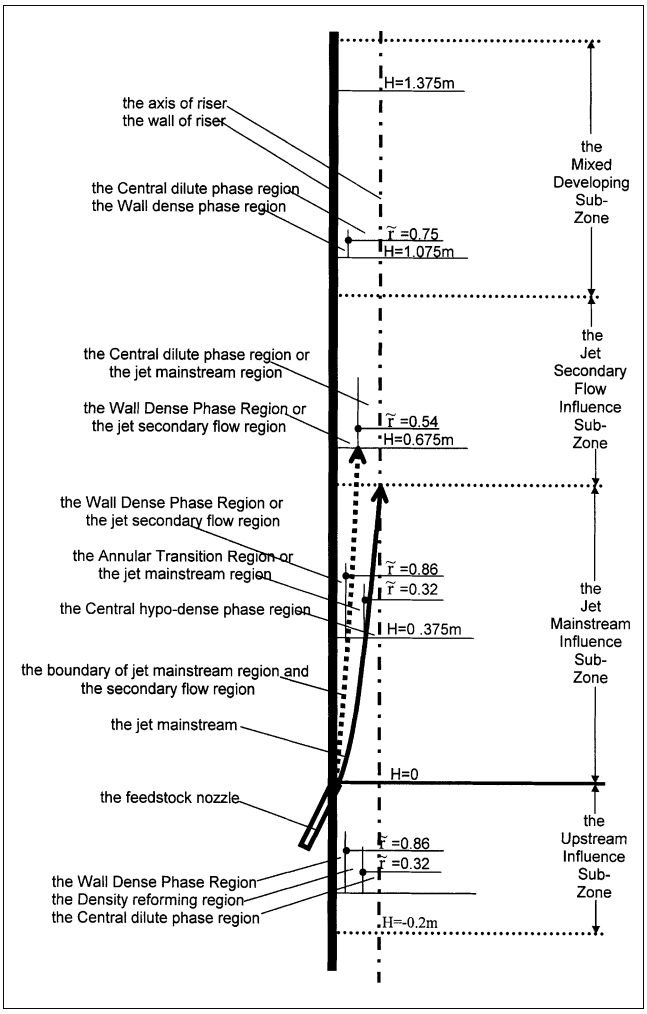

Figure 10. Flow structure in riser feedstock injection zone (not to scale).

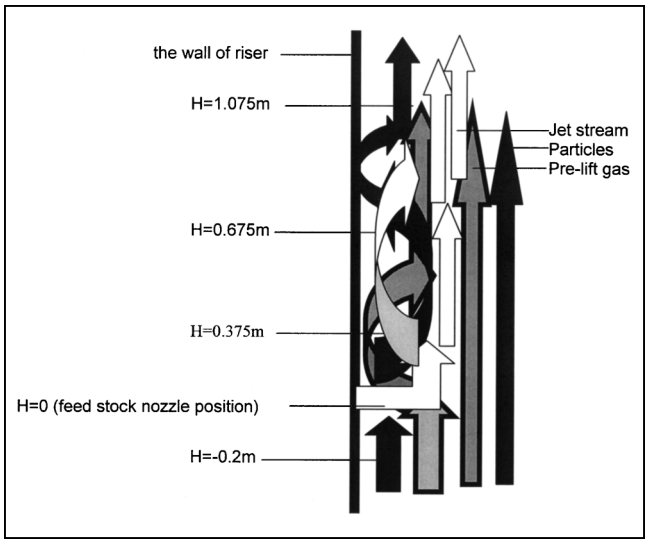

Figure 11. Mixing process in riser feedstock injection zone (not to scale).

cumjacent fluid together with jet mainstream diffusion, the jet secondary flow gradually elongated. At the boundary between the mainstream and the secondary flow, and in the steeper velocity gradient, intense shearing makes the local density distribution gradient much sharper, and then forms three regions in the radial direction, the wall dense-phase region, the annular transition region, and the central hypodense phase region.

With extension of the jet secondary flow and particle performs "the flow round a blunt body," the annular transition region disappears, particles flow transverse intensely and collide frequently, at which point the whole cross section can be divided into the boundary dense region and central dilute region. But in this boundary dense region, the particle backmixing ratio and concentration are much higher than those in the typical annular-core structure.

Next, the jet secondary flow gradually combined with the mainstream and the secondary flow disappeared, at which point the flow field developed toward the typical annular-core structure.

The cause of secondary flow occurrence

In the riser feedstock injection zone, the secondary flow of jet plays a crucial role not only in the mixing of particles with the jet, but in the two-phase flow pattern as well. Thus, a different jet velocity will result in different extents of influence.

In both the jet mainstream influence subzone and the jet secondary flow influence subzone, the radial gradient of the eigenconcentration in the secondary flow region will decrease if the velocity ratio increases. At the same time, the eigenvelocity in the secondary flow region increases with the increase in the velocity ratio. This demonstrates that a larger velocity ratio causes a more intensive secondary flow so that the diffusion of the jet is more rapid and the mixing of the jet with the particles is improved.

The secondary jet flow also greatly affects other flow parameters.

In the secondary flow region of the jet mainstream influence subzone, the mean axial particle velocity increases as the velocity ratio increases, while the variations in the particle backmixing ratio and the local density present the opposite tendency. But in the secondary flow region of the jet secondary flow influence subzone, the particle backmixing ratio increases as the velocity ratio increases, while the mean axial particle velocity and the local density assume the opposite tendency, which is also influenced by the jet secondary flow.

From the preceding discussion, a noticeable point is that a larger velocity ratio will result in a more intensive secondary

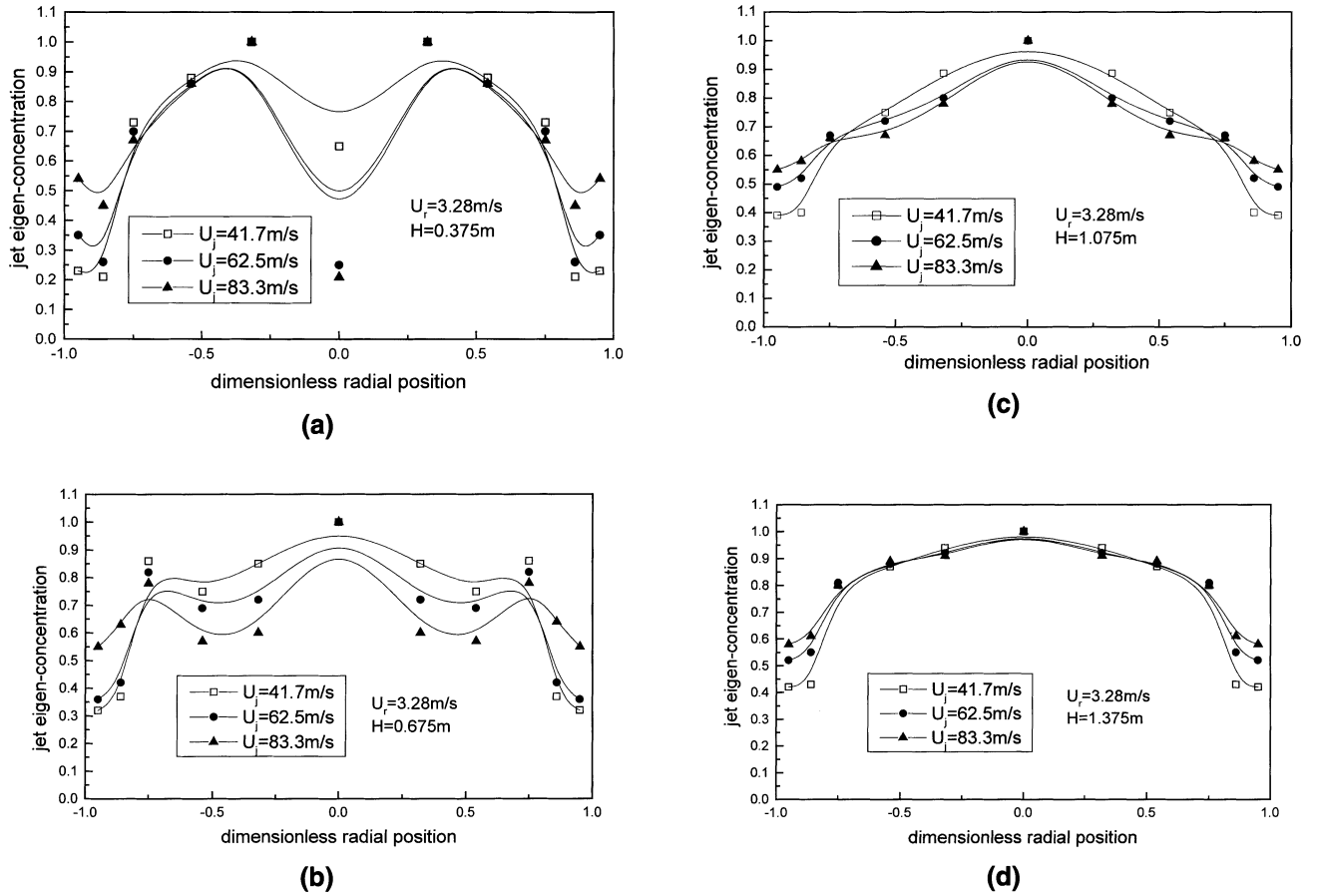

Figure 12. Radial distribution of jet eigenconcentration in four measured sections: (a) 0.375 m above nozzles; (b) 0.675 m above nozzles; (c) 1.075 m above nozzles; (d) 1.375 m above nozzles.

flow of the jet. With the extension of the jet secondary flow, more particles will be carried toward the riser wall, and then more particle collisions will take place.

On the other hand, in the jet mainstream region, both the jet mainstream influence subzone and jet secondary flow influence subzone, the axial particle velocity increases when the velocity ratio increases. But the particle backmixing ratio and the local density present exactly opposite tendencies.

As to the flow parameters in the mixed-developing subzone, they have the same diverse tendencies as those of increased superficial gas velocity, except for jet injection, namely, the particle backmixing ratio, and the local density decreases if the velocity ratio increases both in the wall dense phase region and in the central dilute phase region. But the variation is more complicated for the particle axial velocity: the variation in the axial particle velocity will increase if the velocity ratio increases in the central dilute phase region with the opposite tendency in the wall dense-phase region.

Figures 12–16 clarify the preceding discussion and show that the proper velocity ratio is a decisive factor in influencing the mixing and flow.

The importance of secondary flow is obvious, as it greatly improves the mixing of particles and feedstock jet. On the other hand, because the position of the secondary jet flow corresponds exactly to the particle dense-phase region in which the axial particle velocity is relatively low and backmixing is violent, it is believed to be harmful to the FCC unit. Discovering the cause of the secondary jet flow generation is a key factor in effectively controlling and harnessing it.

The emergence of the secondary jet flow is due to vortices induction. That is to say, the tangential component of vortices $\Omega_\theta = \partial u_r/\partial x_z - \partial u_z/\partial x_r$ will contribute much to the generation of the secondary jet flow. In incompressible single-phase flow, the direction of the velocity induced by vortices can be determined by the right-hand rule, and its intensity obeys the Biot–Savart theorem. But in multiphase flow, the vortices cause the momentum, not the velocity, and this momentum contributes greatly to the transport of two-phase flow in the feedstock injection zone.

A map of the coordinates is shown in Figure 17.

Because of the fact that the intensity of the vortex grows weaker the further it is from the feedstock nozzle, the momentum induced by vortices in region I is toward the riser axis, while the momentum in region II is toward the riser wall. It is the induced momentum in region II that results in the generation of the secondary jet flow. Similarly, the induced momentum in region III is toward the riser axis. It is the influence of these three vortices that determines the process of first the jet secondary flow extension and then in combination with the jet mainstream.

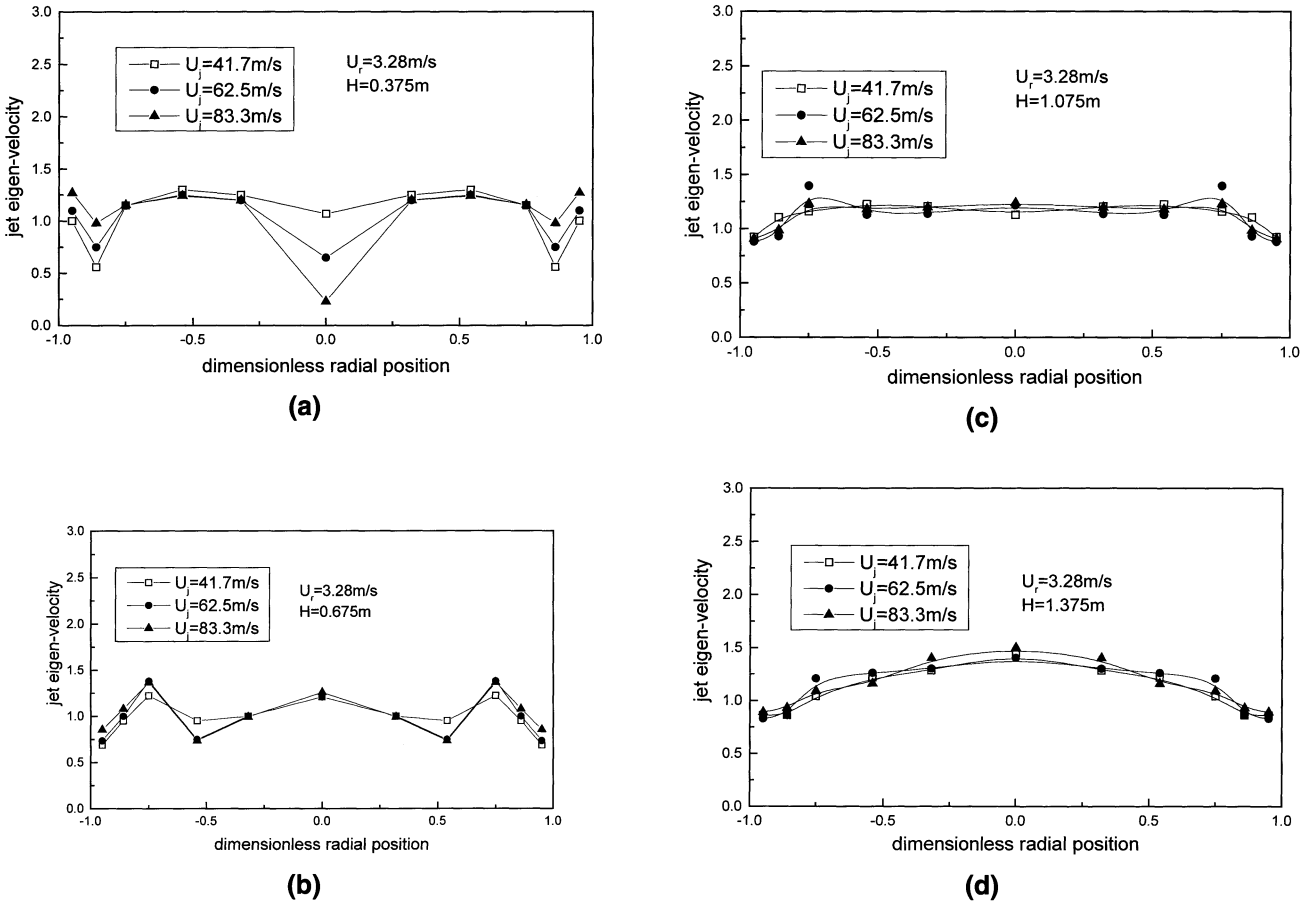

Figure 13. Radial distribution of jet eigenvelocity in four measured sections: (a) 0.375 m above nozzles; (b) 0.675 m above nozzles; (c) 1.075 m above nozzles; (d) 1.375 m above nozzles.

In a similar manner, a particle is also influenced by these three vortices, resulting in particles performing the "the flow round a blunt body" in the jet secondary flow influence subzone, where particles collide with each other exquisitely and the particle backmixing ratio greatly increases.

Theoretical Analysis

As discussed earlier, the two-phase flow in the feedstock injection zone is very complex. It involves the velocity regime, concentration regime, vortices regime of both the gas phase and the solid phase, which makes establishing a predictive model very difficult. Numerical simulation is too complicated to be applied practically in engineering, even as the most comprehensive mathematical description. The main objective of this work is to establish a tractable, predictive mathematical hydrodynamic model that can be employed to describe and characterize all the key flow parameters in the feedstock injection zone. The input parameters considered are limited to the riser operating conditions (solid flux, jet velocity, and superficial prelift gas velocity), the riser geometry, and the physical properties of the gas and solid.

The particle backmixing model

Particle backmixing refers to the phenomenon that inside a riser reactor a portion of the particles flow downward due to collision or the effect of the boundary, while the majority of the particles move upwards, and then fall "back." Those particles flowing downwards unavoidably mix with those moving upwards from the riser bottom, which results in "mixing."

The downflowing particles inevitably result in a longer residue time in the reacting region, which is believed harmful to the whole FCC unit, as discussed earlier. Thus the particle backmixing becomes an important physical phenomenon to understand well.

The map of the particle backmixing model is shown in Figure 18. During a given time period, the flux of the particles flowing upward past this point is $q_u + q_d$, and at the same time the flux of the downflowing particles is q_d, and therefore the net flux past this point is q_u. The fluxes q_u and q_d can be determined, respectively, by measured particle velocities v_u and v_d, multiplied by the measured number of particles flowing upwards and downwards.

Thus the particle backmixing ratio can also be described as $q_d/(q_u + q_d)$, while the mean axial velocity of particles can be expressed as

$$\nu = \frac{q_u + q_d - q_d}{n_u + n_d} = \left(\frac{q_u + q_d}{n_u + n_d}\right)\left(\frac{q_u + q_d}{q_u + q_d} - \frac{q_d}{q_u + q_d}\right). \quad (5)$$

Hypothesis. 1. In the riser feedstock injection zone, the axial density gradient is supposed to be $\partial\rho/\partial z \neq 0$.

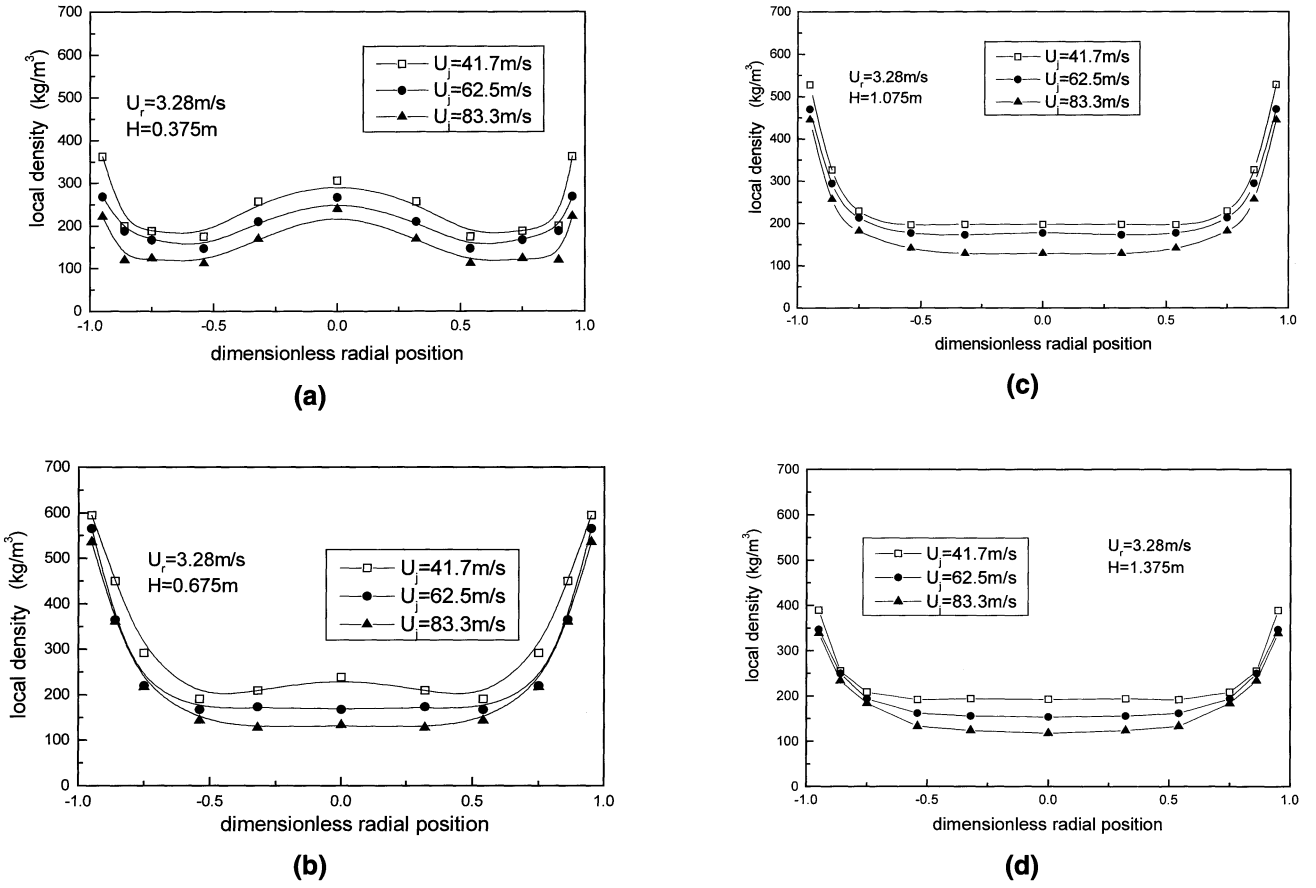

Figure 14. Radial distribution of local density in four measured sections: (a) 0.375 m above nozzles; (b) 0.675 m above nozzles; (c) 1.075 m above nozzles; (d) 1.375 m above nozzles.

2. The increase in the particle backmixing ratio is equivalent to the decrease in the axial density gradient under the same solid flux and same mean particle axial velocity. The extreme condition is when the particle backmixing ratio α is close to 1, which means the net upward flux tends to 0, so as the particle velocity also approaches 0, the density gradient must approach 0, which can be deduced by the continuity equation easily. On the other hand, when α is close to 0, and the whole effect of particle acceleration or deceleration should be employed to change the axial density distribution, the density gradient presents a maximum.

3. The closer to each other the values of the upward and downward flux are, the more intense is the extent of mixing between the particles flowing upwards and downwards, and the flatter the axial density gradient profile.

Relation of the Generalized-Peclet Number Pe to the Particle Backmixing Ratio α. The diffusion equation for the solid phase in the cylindrical coordinate is given as follows:

$$\upsilon_r \partial\rho/\partial r + \upsilon_\theta \partial\rho/r\partial\theta + \upsilon_z \partial\rho/\partial_z = D_j\left[\partial(r\partial\rho/\partial r)/r\partial r + \partial^2\rho/r^2\partial\theta^2 + \partial^2\rho/\partial z^2\right], \quad (1)$$

where the density term ρ can be determined by $\rho = \rho_p \epsilon_p$.

The radial and tangential parameters can be omitted, as particle backmixing occurs only in the axial direction. Introducing a characterizing axial length δh to make the equation dimensionless, and supposing $\tilde{z} = z/\delta h$, then Eq. 1 can be simplified as

$$\frac{d\rho}{d\tilde{z}} = Ce^{\upsilon_z h\tilde{z}/D_j}, \quad (6)$$

where C is a constant.

Equation 6 indicates that the bigger the diffusion coefficient D_j is, which means the more intense the extent of particle diffusion is, the flatter the axial density gradient is. It also means the extent of "mixing" between the upward and downward particle flows is more intense and the backmixing ratio of the particles is larger.

Thus, the diffusion coefficient, D_j, can be used to correlate with the particle backmixing ratio.

The exponential term $\upsilon_z h/D_j$ in Eq. 6 is defined as the generalized Peclect number and is denoted by the dimensionless variable, *Pe*. This generalized Peclet number, *Pe*, can reflect the extent of particles mixing. But it differs from the common Peclet number because in the generalized Peclet number, the diffusion coefficient, D_j, represents the extent of mixing, and its diffusion potential is pressure that is transformed by gravity rather than by the concentration gradient. In fact, in a gas–solid circulating fluidizing bed system, the gravity itself cannot act as a diffusion potential unless it is converted into pressure $\delta p = \rho g \delta h$.

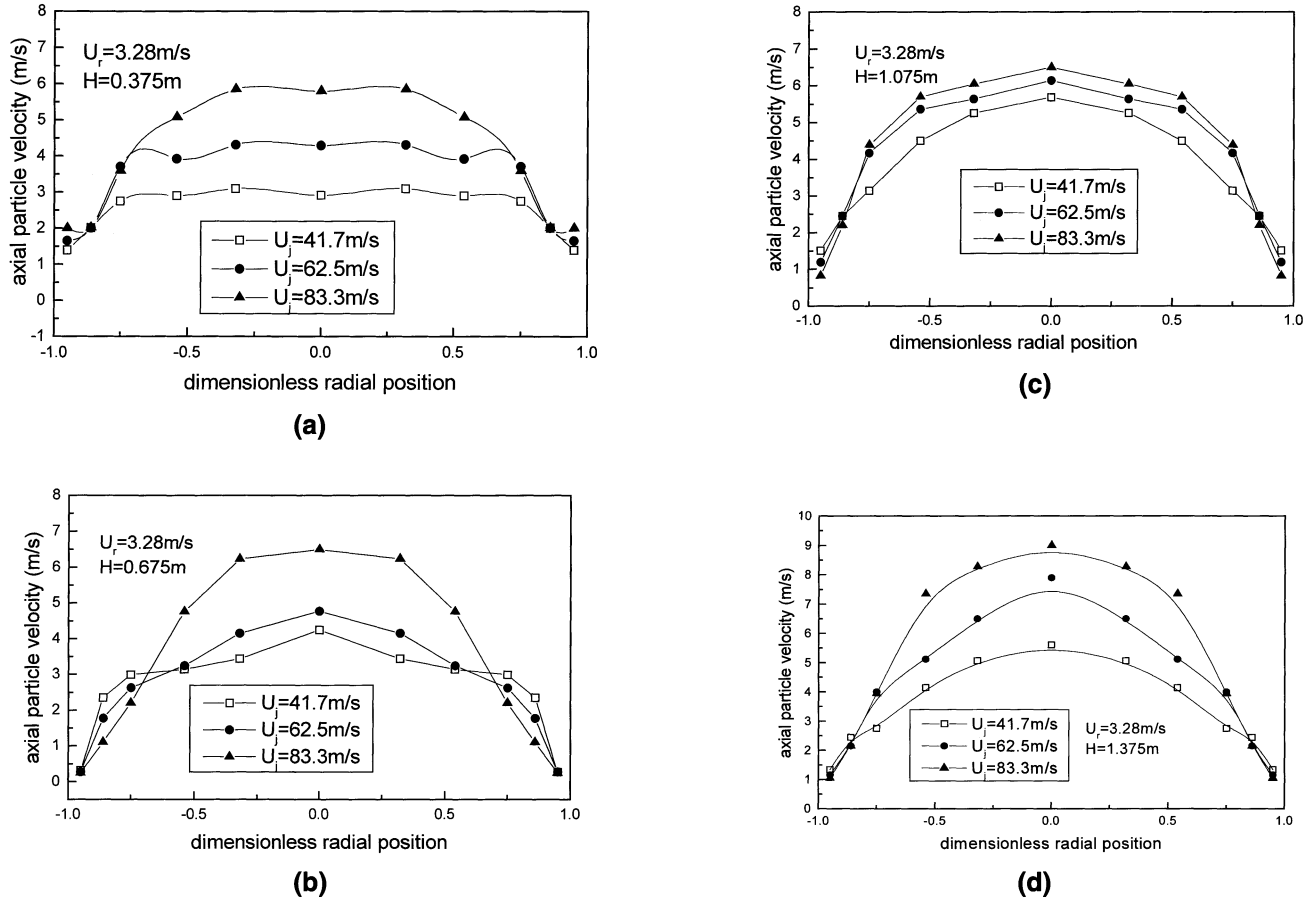

Figure 15. Radial distribution of axial particle velocity in four measured sections: (a) 0.375 m above nozzles; (b) 0.675 m above nozzles; (c) 1.075 m above nozzles; (d) 1.375 m above nozzles.

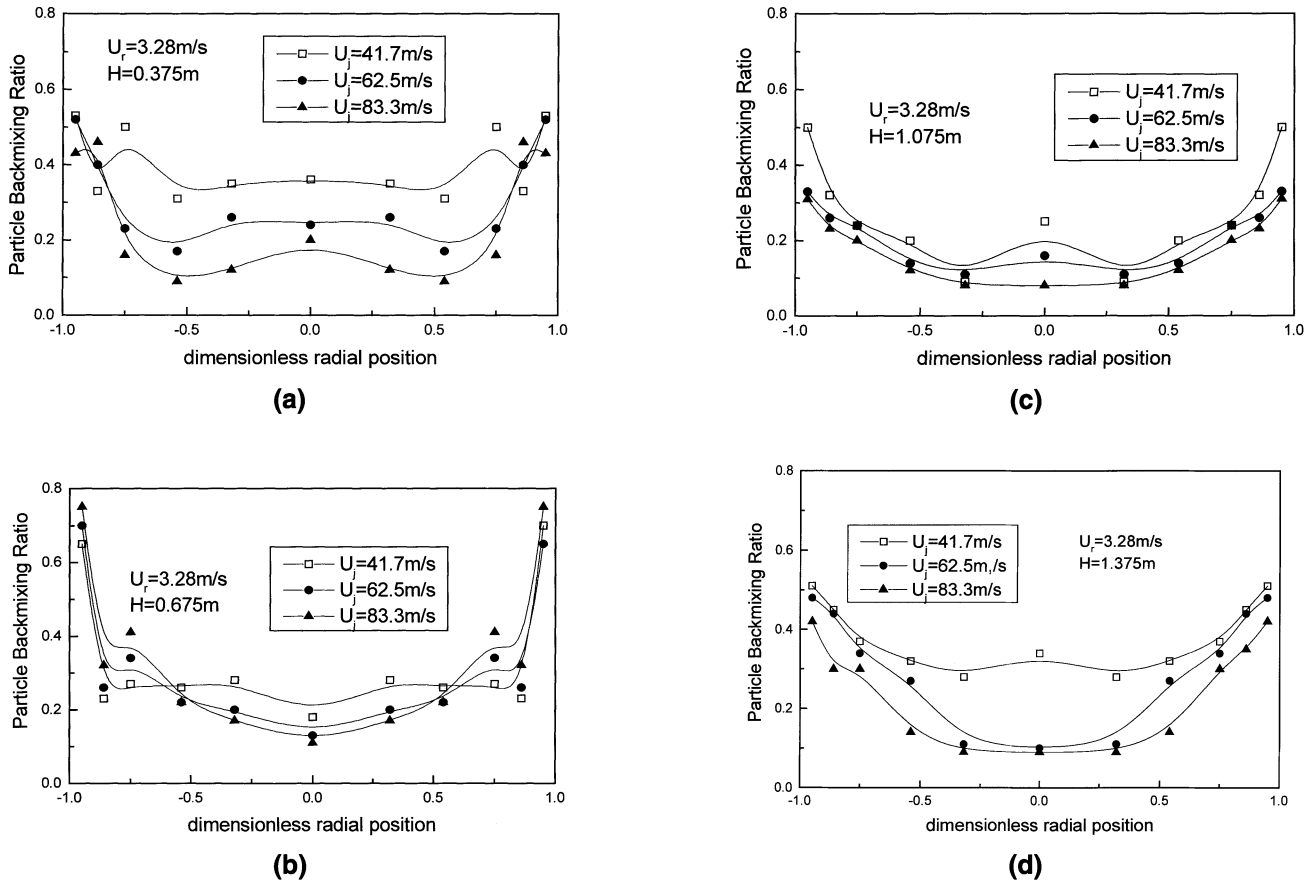

Figure 16. Radial distribution of particle backmixing ratio in four measured sections: (a) 0.375 m above nozzles; (b) 0.675 m above nozzles; (c) 1.075 m above nozzles; (d) 1.375 m above nozzles.

In this work, at any position in the riser feedstock injection zone, the particle backmixing ratio $\alpha \leq 1$, namely, the particle velocity, is upward as a whole.

When particle backmixing is absent at a given position, two-phase flow assumes plug flow, which means $D_j = 0$. On the other hand, when particle backmixing is complete, $D_j \rightarrow -\infty$. The introduction of the minus sign here shows that the direction of particle velocity and of particle backmixing are exactly the opposite to each other.

From a mathematical point of view, the relations between Pe and α can be summarized as follows:

1. If $\alpha = 0$, that is, the value of q_d equals 0, then the diffusion coefficient, D_j, which characterizes the mixing extent, also equals 0, so it can be deduced that Pe approaches $-\infty$, according to the definition of Pe;

2. If $\alpha = 1$, that is, the value of q_u equals 0, then the diffusion coefficient, D_j, which characterizes the mixing extent,

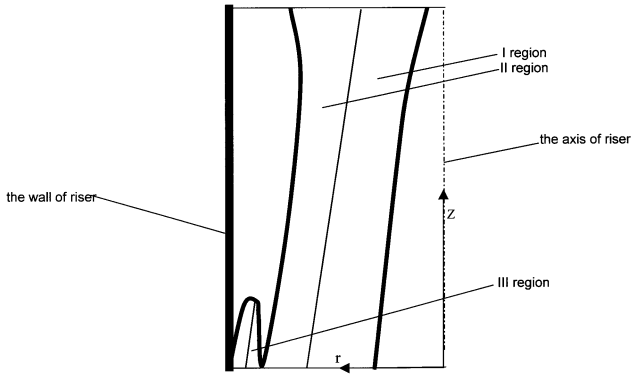

Figure 17. Coordinate to account for the arise of the jet secondary flow.

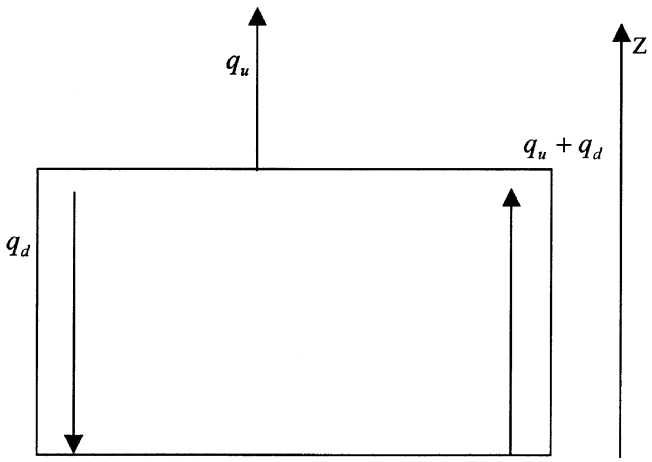

Figure 18. Particle backmixing model.

tends to ∞, and the mean particle velocity is also equal to 0, so Pe is close to 0;

3. The larger the value of α is, the smaller the v_z in the numerator is, and the larger the D_j in the denominator is. That is to say, the generalized Peclet number, Pe, decreases as α increases.

Thus the relation between Pe and α can be obtained by the analysis given earlier:

$$Pe = |\ln(k\alpha)|, \tag{7}$$

when $\alpha \leq 1$, and

$$\alpha = 1/k \exp(Pe). \tag{8}$$

When the particle diffusion potential is the pressure transformed by gravity (Liu, 1993),

$$-D_j \frac{\partial \rho}{\partial z} = A\rho t \left(\frac{1}{\rho_g} - \frac{1}{\rho_p} \right) \frac{\partial p}{\partial z},$$

then

$$D_j = k_1 \rho, \tag{9}$$

that is,

$$Pe = v_z / k_1 \rho, \tag{10}$$

then Eq. 8 can be converted into

$$\alpha = 1/k \exp(v_z/k_1 \rho) = 1/k \exp(Pe), \tag{11}$$

where

$$\begin{cases} k_1 = 0.07246 \\ k = 2.75 \quad r/R \leq 0.86 \\ k = 1.964 \quad r/R > 0.86 \end{cases}.$$

Figure 19 shows the comparison between the measured and computed values under a typical operating condition with Eq. 11 for the particle backmixing ratio. It shows good agreement between Eq. 11 and the experimental results.

It also shows that the particle backmixing ratio decreases with an increase in particle velocity and voidage, which is in agreement with the actual situation.

Correlation of Particle Axial Velocity. The significance of introducing the generalized Peclet number Pe is self-evident.

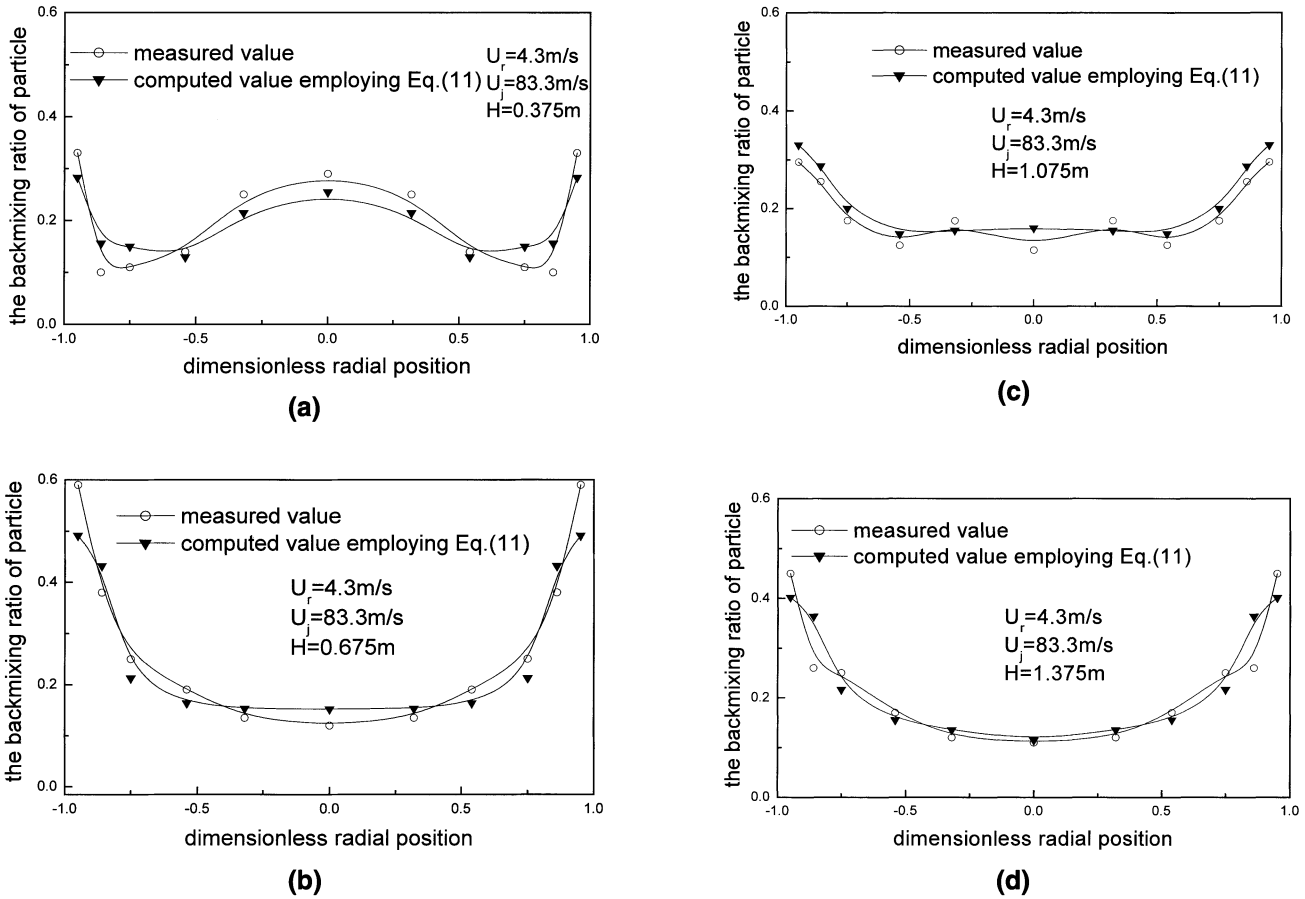

Figure 19. Measured vs. computed value using Eq. 11 for the particle backmixing ratio: (a) 0.375 m above nozzles; (b) 0.675 m above nozzles; (c) 1.075 m above nozzles; (d) 1.375 m above nozzles.

This Pe is not only a function of particle axial velocity, but a function of local density as well, and the distributions of these two parameters in the riser feedstock injection zone will greatly influence the catalytic reaction. Thus, introduction of Pe makes the flow of the solid phase more predictable.

To compute the particle velocity and local density, however, some other constraints must be introduced.

By introducing a parameter,

$$\beta_1 = \frac{q_u + q_d}{n_u + n_d},$$

the mean particle axial velocity can be expressed as

$$v_z = \beta_1(1-\alpha), \tag{12}$$

where β_1 is a characterizing velocity of the upward particle flow.

By analyzing 495 groups of experimental data in five different cross sections, it is found that in each measured section, the parameter β_1 is only a function of position and is independent of the operating condition. That is to say, the value of the particle axial velocity in a given position is determined only by the condition that the location function β_1 and the particle backmixing ratio α were given. In fact, the particle backmixing ratio itself is undoubtedly a function of such operating parameters as nozzle velocity and particle flux.

In order to improve fitting, a new parameter $\beta = 10/\beta_1$ is introduced and is named the particle velocity coefficient.

But flow in the riser feedstock injection zone is highly complex. The particle velocity coefficient, β, varies axially and radially. Moreover, because the riser feedstock injection zone is a confined space, the asymptotic method for this type of flow is inapplicable. Therefore, the particle velocity coefficient cannot be expressed as a function of r/z^m (where m can be any real number).

Distribution of β in five different measured cross sections is accomplished by fitting experimental data. The values of β in other cross sections have to be determined by means of interpolation:

$$\beta = \sum_{i=0}^{6} a_i \tilde{r}^i. \tag{13}$$

Therefore, the particle axial velocity in a certain position can be worked out with Eq. 14 if the value of the particle velocity coefficient, β, and particle backmixing ratio, α, are given:

$$v_z = 10(1-\alpha)/\beta. \tag{14}$$

Correlation of Generalized Peclet Number Pe. Unlike the particle velocity coefficient, β, the generalized Peclet number, Pe, is not only a function of positional coordinates, but also a function of the operating parameters.

But because of the extreme complexity of the flow field and the tendency of Pe to be nonuniform in different positions, this article presents the distributions of Pe in five different measured cross sections just like the particle velocity coefficient, β, being computed. In other sections, the value of Pe has to be estimated by interpolation.

The first fitting result shows that the operating parameters most related to Pe are particle flux, G_s; the ratio of the nozzle jet velocity and the superficial prelift gas velocity, λ; the total superficial gas velocity, U_z, in the riser into which the nozzle jet gas has been injected; and the radial position, $\tilde{r}$.

The Pe expression can be written as follows, just like that of the Nusselt number in heat transfer of a small amount of cool gas spouted into the gas with different temperatures and velocities in an infinite space:

$$Pe = b_0\left[(Re_p)^{0.5}\right]^{b_1}(U_z/v_t)^{b_2}\lambda^{b_3} \tag{15}$$

$$Re_p = \frac{\rho U_z d_p}{\mu}$$

$$v_t = (\rho_p - \rho_g) d_p^2 g/18\mu$$

$$\lambda = U_j/U_r.$$

For more detailed information about the values of b_0, b_1, b_2, b_3 in Eq. 15, which are determined by fitting experimental data, the reader should consult Fan's (2000).

The preceding analysis clearly shows the following computational process of the particle backmixing model.

First, the generalized Peclet number, Pe, by Eq. 15, and the particle velocity coefficient are worked out by Eq. 13, after which the calculation procedure follows in the order: the particle backmixing ratio, α, by Eq. 11, the axial particle velocity by Eq. 14, and finally the local density ρ by Eq. 10. The whole process can be expressed as follows:

The generalized Peclet number, Pe → the particle backmixing ratio α / particle velocity coefficient β

→ axial particle velocity v_z / coefficients k, k_1 → local density ρ.

Simplified model to compute the distribution of nozzle jet in riser cross section

Analysis for Influential Factors and Determination of Correlative Parameters. In general, the particle flux, jet velocity, superficial prelift gas velocity, and the dimensions of the riser will greatly affect the distribution of the nozzle jet in the riser cross section.

But the relaxation times of gas–gas and gas–solid are enough different that the "affinity" of jet–particle is much less than that of the jet–prelift gas. Thus the extent of the influence of each factor is quite distinct.

When using two-phase flow model, the viscosity stress and turbulent stress are omitted because of their relatively small influence during the mixing process. Thus radial momentum equations of the jet gas and of prelift gas are as follows:

$$\frac{\partial}{\partial z}(\rho_j \epsilon_j u_{jr} u_{jz}) + \frac{\partial}{r\partial r}\left(r\rho_j \epsilon_j u_{jr}^2\right) = -\epsilon_j \frac{\partial p}{\partial r} - \frac{\rho_j \epsilon_j \rho_r \epsilon_r}{(\rho_j \epsilon_j + \rho_r \epsilon_r)}\left(\frac{u_{jr} - u_{rr}}{t_{jr}}\right) - \frac{\rho_j \epsilon_j \rho_p \epsilon_p}{(\rho_j \epsilon_j + \rho_p \epsilon_p)}\left(\frac{u_{jr} - v_{pr}}{t_{jp}}\right) \tag{16}$$

$$\frac{\partial}{\partial z}(\rho_r \epsilon_r u_{rr} u_{rz}) + \frac{\partial}{r\partial r}\left(r\rho_r \epsilon_r u_{rr}^2\right) = -\epsilon_r \frac{\partial p}{\partial r} + \frac{\rho_j \epsilon_j \rho_r \epsilon_r}{(\rho_j \epsilon_j + \rho_r \epsilon_r)}\left(\frac{u_{jr} - u_{rr}}{t_{jr}}\right) - \frac{\rho_r \epsilon_r \rho_p \epsilon_p}{(\rho_r \epsilon_r + \rho_p \epsilon_p)}\left(\frac{u_{rr} - v_{pr}}{t_{rp}}\right). \tag{17}$$

The first subscript letters j, p, r represent, respectively, jet gas, particle phase, and prelift gas, while the second letters represent directions of vectors.

When the relaxation time between the nozzle jet gas and prelift gas is very short, Df/Dt must be $\ll f/t$. If these two equations are transformed properly, the partial differential equation can be converted into an algebraic equation and become the multiphase flow diffusion model:

$$u_{jr} - u_{rr} = \left[-\epsilon_j \frac{\partial p}{\partial r} + \epsilon_r \frac{\partial p}{\partial r} - \frac{\rho_j \epsilon_j \rho_r \epsilon_r}{(\rho_j \epsilon_j + \rho_r \epsilon_r)}\left(\frac{u_{jr} - u_{rr}}{t_{jr}}\right)\right] t_{jr}. \tag{18}$$

Equation 18 indicates that the volume faction distribution is determined by relaxation time, discrepancy of radial veloc-

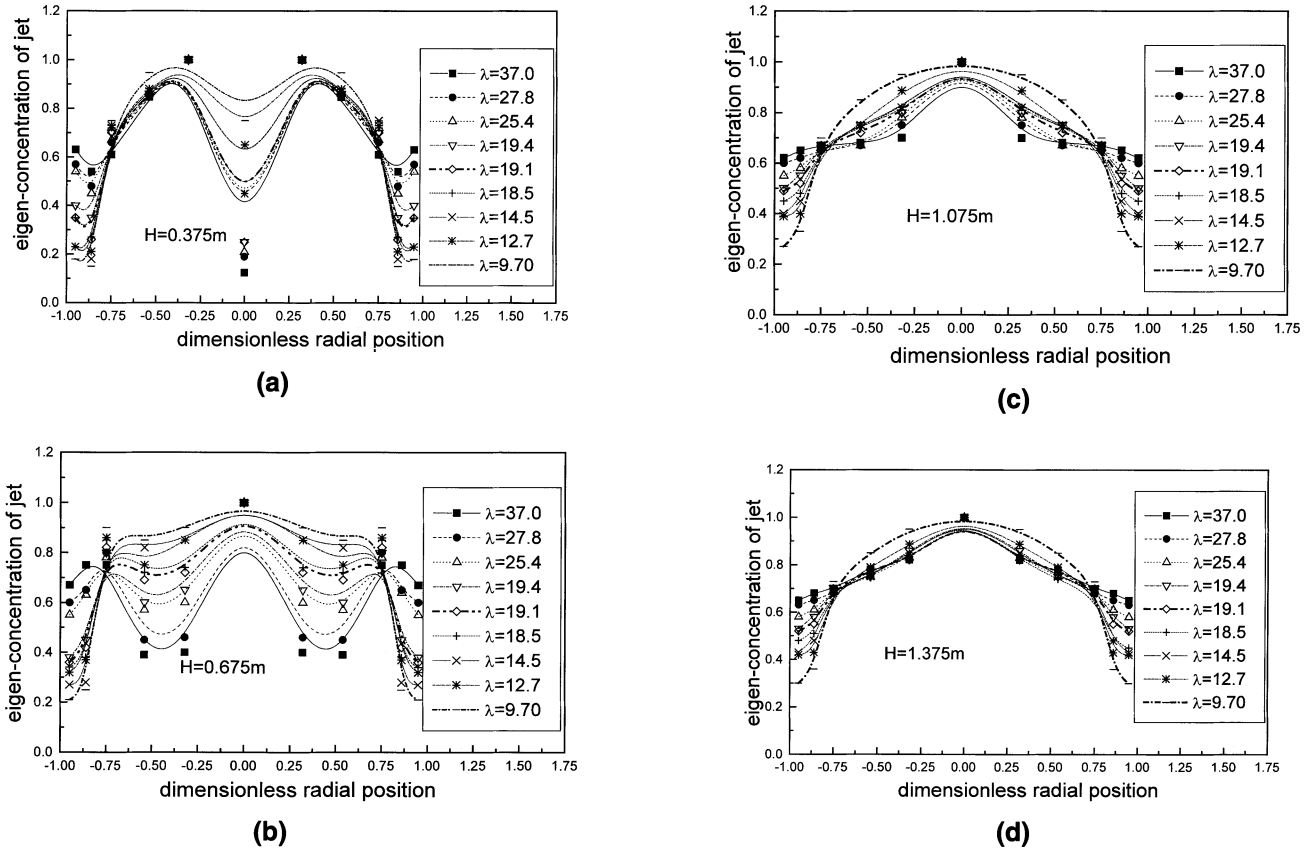

Figure 20. Radial distribution of jet eigenconcentration varying with the velocity ration: (a) 0.375 m above nozzles; (b) 0.675 m above nozzles; (c) 1.075 m above nozzles; (d) 1.375 m above nozzles.

ity, and pressure component. But these parameters cannot be measured in the riser because of the limitation of the experimental method. This article introduces the hypothesis that these parameters are determined only by the initial conditions of the prelift gas and of the nozzle jet. Thus, the cross-sectional distribution of the jet gas is determined only by the ratio of the prelift gas and nozzle jet velocities.

Figure 20 shows that the preceding hypothesis is reasonable to some extent, and at least indicates that the velocity ratio is the main key factor in determining the jet flow parameter distribution in the riser cross sections, while other factors such as particle flux play only a subsidiary role.

Therefore, in this article, when correlating the distribution of jet concentration in the riser cross sections, the only factor we are concerned with is the velocity ratio.

Cross-Sectional Distribution of Jet Eigenconcentration. In the jet mainstream influence subzone and the jet secondary flow influence subzone, jets mix intensively with the flow coming from the prelift zone. The cross-sectional distribution of the jet eigenconcentration is very complex, even more complex than that of the generalized Peclet number, *Pe*. The radial distribution of the jet eigenconcentration is very different in different cross sections due to the influence of vortices; even their varying tendency is entirely diverse.

In this article the radial gradient of the jet eigenconcentration, $d\bar{C}/d\tilde{r}$, varies with the velocity ratio, λ, in five different measured cross sections, the same as when the velocity coefficient, β, and the generalized Peclet number, *Pe*, are computed. However, the value of $d\bar{C}/d\tilde{r}$ has to be estimated by interpolation in other sections.

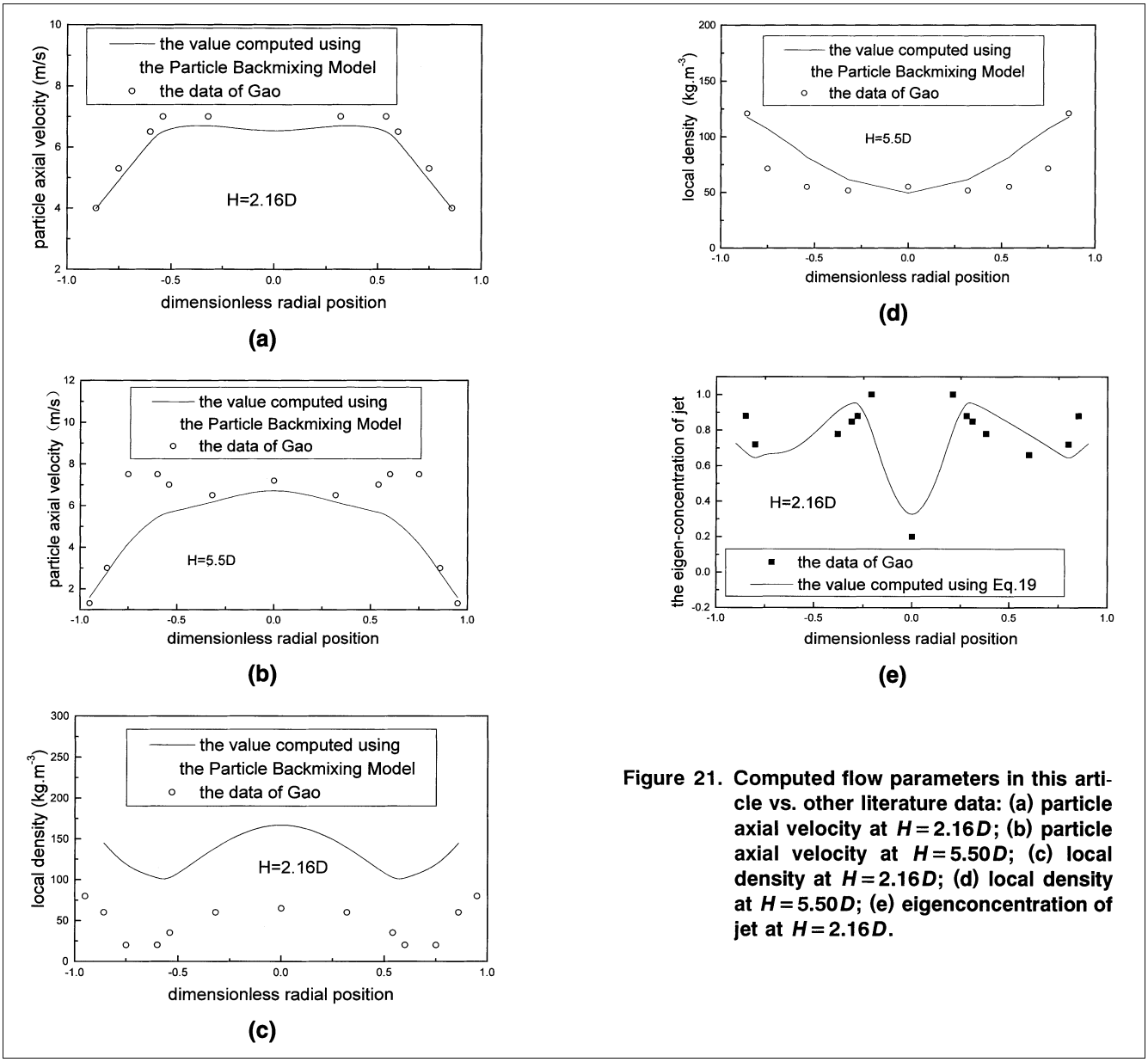

Figure 21. Computed flow parameters in this article vs. other literature data: (a) particle axial velocity at $H = 2.16D$; (b) particle axial velocity at $H = 5.50D$; (c) local density at $H = 2.16D$; (d) local density at $H = 5.50D$; (e) eigenconcentration of jet at $H = 2.16D$.

The radial eigenconcentration distribution of jet gas in different sections can be expressed as follows:

$$d\bar{C}/d\tilde{r} = c_0 \lambda^{c_1} r^{c_2}. \quad (19)$$

For more detailed information about the values c_0, c_1, c_2 in Eq. 19, which are obtained by fitting experimental data, the reader can refer to Fan (2000).

Validity of the Computational Methods Introduced in This Article. As related research, and especially experimental research on the flow pattern in the feedstock injection zone of the FCC riser, is very scarce, comparable data are almost inaccessible. In order to test the validity of Eq. 19 and the particle backmixing model, the results computed by the method introduced in this article have to be compared with numerical simulation from other literature.

Figure 21 compares the computed values using Eq. 19 and the particle backmixing model with the numerical simulation results by Gao (1997). It also shows a passable agreement between them. At least their distribution tendencies are entirely coincident.

Because the objects computed are industrial devices in Gao (1997), some discrepancies must exist between the industrial and experimental conditions. Moreover, the initial conditions adopted by Gao (1997) are in disagreement with those of the experiment, such as its hypothesis of the uniform inlet boundary condition. Furthermore, the jet density in industrial conditions is higher than that in experimental conditions, so the influence regime lasts longer than that of the experimental condition. According to the data of Gao (1997), the velocity maximum is not located at the riser axis, but shifts to $\tilde{r} = 0.5 \sim 0.7$ at a height of 5.5D. On the other hand, the annular-core structure appears at a height of 3.6D in the experimental model.

At a height of 2.16D, according to the data of Gao (1997), the local density distribution is in disagreement with that computed by the particle backmixing mode. This discrepancy is caused by the hypothesis of uniform inlet boundary condition in Gao's simulation (1997). In fact, the inlet boundary condition is quite different from the uniform distribution, as shown in Figure 9. Then more particles will be blown toward the riser's central area by jet than in that computed by Gao (1997). Furthermore, the density near the riser wall will be higher than that provided the uniform inlet boundary condition. So the computed density in Gao (1997) is lower than when using the particle backmixing model.

At a height of $H = 5.5$D, the flow takes on the typical annular-core structure, so that good agreement is obtained by these two computational methods, respectively.

From the preceding analysis by the particle backmixing model, some initial conditions can be modified to improve the precision of the numerical simulation to some extent.

Conclusions

1. The whole prelift zone can be divided into three subs from bottom to top in the axial direction. They are the mixing accelerating subzone, the uniform accelerating subzone, and the fully developed subzone. The mixing accelerating subzone can be described as a typical three-dimensional flow field, the uniform accelerating subzone is a typical two-dimensional flow area, while the fully developed subzone is characterized as a one-dimensional flow region.

2. The best installation position for feedstock should be located at the uniform accelerating subzone, which can be conducive to the contact and mixing between catalysts and feed oil.

3. The mixing process and flow characteristics in the feedstock injection zone can be well described by using the new parameters introduced in this article, such as particle backmixing ratio, jet eigenconcentration, and jet eigenvelocity.

4. The experimental results indicate that a secondary jet flow takes place in the riser feedstock injection zone. The secondary flow extends at first, and then emerges into the mainstream when feedstock is injected into the riser. It also shows that the jet secondary flow greatly influences the flow parameters, such as the distributions of local density and particle backmixing.

5. The occurrence and development of jet secondary flow in the feedstock injection zone can be interpreted by the theory that vortices induce velocity.

6. When feedstock is injected into the riser, the flow feature is much different from the typical annular-core structure. The whole feedstock injection zone can be divided into four subzones according to the flow behavior of the jet and of the solid phase. Each subzone can be further divided into two or three regions in the radial direction. Detailed positions of each subzone and each region are given.

7. This article indicates that the mismatch of catalyst concentration distribution with jet concentration distribution is the main cause for the nonuniform contact between catalyst and feedstock.

8. From this article, the uppermost reason for charring may be the particles performing "the flow round a blunt body" and extension of the jet secondary flow, rather than the prevalent viewpoint of "feedstock jet impinging on the opposite riser wall of the atomizing nozzle."

9. Given the fact that the backmixing of particles is inevitable in the riser, two new parameters, generalized Peclet number, Pe, and particle velocity coefficient, β, are defined. Furthermore, a particle backmixing model, $\alpha = 1/k \exp(Pe)$ and $\beta = f(\tilde{r})$ is given to facilitate the description of the particle flow feature in the riser feedstock injection zone.

10. The velocity ratio is the most crucial factor in determining the jet concentration distribution in the riser cross sections, while other operating parameters play only a minor role, according to the experimental results and the multiphase flow diffusion equation.

11. By using the simplified model introduced in this article, more practical initial conditions are provided so that the precision of the numerical simulation can be improved.

Acknowledgments

The authors gratefully acknowledge the financial support from the CNPC (China Nature Gas and Petroleum Corporation) and the SINOPEC (China Petrochemical Corporation) for this study.

Notation

Ar = Archimedes number $[\rho_g(\rho_p - \rho_g)d_p^3 g]/\mu^2$
C = concentration
C_i = tracer concentration sampled by a sampling tube

$\bar{C}$ = $\lambda[(C_i/\Sigma C_i)\ (Q_j/(Q_j + Q_r))]$ = the eigenconcentration of jet
D = diameter of riser, m
D_j = diffusion coefficient, m^2/s
Fr = Froud number $(U_r^2/d_p g)$
g = acceleration of gravity, m/s^2
G_s = particle flux, $kg/m^2 s$
h = characterizing axial dimension, m
H = height above gas distribution, m
H_a = particle acceleration length in prelift zone
H_j = the proper location to fix feedstock nozzles
k = coefficient
k_1 = coefficient
n_d = number of the particles whose velocity is downward
n_u = number of the particles whose velocity is upward
p = pressure, Pa
Pe = generalized Peclet number
q = entries flux of particle, entries/s
Q = flux of gas, m^3/s
Q_j = gas flux of four jets
Q_r = gas flux of the prelift gas
Re_g = superficial Reynolds number of prelift gas $(U_r D\rho_g/\mu)$
Re_p = superficial Reynolds number of particle $(G_s d_p/\mu)$
r = radial
t = relax time, the mean residency time of the trace, s
u = velocity of gas phase, m/s
u_r = velocity of prelift gas, m/s
u_j = velocity of nozzle jet gas, m/s
u_e = eigenvelocity of the jet, m/s
U_r = superficial velocity of prelift gas, m/s
U_j = superficial velocity of nozzle jet injection, m/s
U_z = superficial gas velocity when nozzle jet has injected in the riser, m/s
v = particle velocity, m/s
v_t = terminal velocity of particle, m/s
v_d = mean velocity of particles whose velocity is downward
v_u = mean velocity of particles whose velocity is upward
Z = axial height, m

Greek letters

α = particle backmixing ratio
β = particle velocity coefficient, s/m
λ = ratio of nozzle jet velocity and superficial prelift gas velocity, $\lambda = U_j/U_r$
ϵ = volume fraction
ρ = local density, kg/m^3
θ = tangential
μ = viscosity, Pa·s

Superscripts and subscripts

$\sim$ = dimensionless
j = nozzle jet gas
p = particle
Z = axial
r = radial; prelift
θ = tangential

Literature Cited

Agillion, J., K. Shakourzadeh, and P. Guigon, "Hydrodynamic Behavior of Circulating Fluidized Bed with Secondary Air Injection," CFB-5 Preprints, DGS4 1-6 (1996).

Albrecht, A., O. Simonin, D. Barthod, and D. Vedrine, "Multidimensional Numerical Simulation of the Liquid Feed Injection in a Industrial FCC Riser," CFB-10 Preprints, 349 (2001).

Andreopoulos, J., and W. Rodi, "Experiment Investigation of Jets in a Crossflow," *J. Fluid Mech.*, **158**, 93 (1984).

Arena, U., A. Marzocchella, V. Bruzzi, and L. Massimilla, "Mixing Between a Gas-Solid Suspension Flowing in a Riser and a Lateral Gas Stream," CFB-4 Preprints, 660 (1993).

Brereton, C. M., and J. R. Grace, "Microstructure Aspects of the Behavior of Circulating Fluidized Beds," *Chem. Eng. Sci.*, **48**, 2565 (1993).

Chen, L. B., and H. Weinstein, "Shape and Extent of the Void Formed by Horizontal Jet in Fluidized Bed," *AIChE J.*, **39**, 1901 (1993).

Crabb, D., and J. H. Whitelaw, "A Round Jet Normal to a Crossflow," *Trans. ASME I: J. Fluid Eng.*, **103**, 142 (1981).

Fan, Y. P., "The Gas-Solid Two-Phase Flow in the FCC Riser," PhD Thesis, Univ. of Petroleum, Beijing (2000).

Gao, J. S., "Numerical Simulation on the Flow, Heat-Transfer, and Reaction in the Catalytic Cracking Riser Reactors," PhD Thesis, Univ. of Petroleum, Beijing (1997).

Keffer, J. F., and W. D. Baines, "The Round Turbulent Jet in a Cross Wind," *J. Fluid Mech.*, **15**, 481 (1963).

Kozin, B. E., and A. P. Baskakov, *Khim. Tekhnol. Topl. Masel*, **3**, 4 (1967).

Liu, D.Y., *Fluid Dynamics of Two-Phase System*, Higher Education Press, Beijing (1993).

Lummi, A. P., and A. P. Baskakov, *Khim. Prom.*, **43**(7), 522 (1967).

Merry, J. M. D., "Penetration of Horizontal Gas Jet into a Fluidized Bed," *Trans. Int. Chem. Eng.*, **49**, 189 (1971).

Miller, A., and D. G. Gidaspow, "Dense, Vertical Gas-Solid Flow in a Pipe," *AIChE J.*, **38**(11), 1801 (1992).

Moussa, Z. M., and R. I. Sykes, "The Near Field in the Mixing of a Round Jet With a Cross Stream," *J. Fluid Mech.*, **80**, 49 (1977).

Needham, D. J., N. Riley, and J. H. B. Smith, "A Jet in Crossflow," *J. Fluid Mech.*, **188**, 159 (1988).

Sergio, L., V. Coelho, and J. C. R. Hunt, "The Dynamics of the Near Field of Strong Jets in Crossflows," *J. Fluid Mech.*, **200**, 95 (1989).

Shakhova, N. A., and G. A. Minayev, "Aerodynamics of Jet Discharge into Fluidized Bed," *Heat Transfer Sov. Res.*, **4**, 133 (1968).

Subramaniam, K., "Three Dimensional Temporal Instability of Compressible Gas Jet Injected in Liquids," *AIAA J.*, **37**, 202 (1999).

Svensson, A., F. Johnsson, and B. Leckner, "Bottom Bed Regime in a Circulating Fluidized Bed Boiler," *Int. J. Multiphase Flow*, **22**, 1187 (1996).

Thelogs, K. N., I. D. Nikou, A. I. Lygeros, and N. C. Markatos, "On the Simulation of Fluid Catalytic Cracking Riser-Type Reactors," CFB-5 Preprints, MSS5 1−6 (1996).

Wang, Q. J., *Conduction Heat and Mass Transfer*, Xi'an JiaoTong University Press, Xi'an (1991).

Xuereb, C., C. Laguerie, and T. Baron, "Etude du Comportement de jets Continus Horizontaux ou Inclines Introduits dans un Lit Fluidise pan un Gaz, Deuxieme partie: Profiles de Vitesse du vitesse du Gaz dans les jets Horizontaux," *Powder Technol.*, **64**, 271 (1991a).

Xuereb, C., C. Laguerie, and T. Baron, "Etude du Comportement de jets Continus Horizontaux ou Inclines Introduits dans un Lit Fluidise pan un Gaz: I. Morphologie des Jets," *Powder Technol.*, **67**, 43 (1991b).

Yong, J. C., N. Won, and S. D. Kim, "Effect of Secondary Air Injection on Axial Solid Holdup Distribution in a Circulating Bed," *J. Chem. Eng. Jpn.*, **27**, 158 (1993).

Zens, F. A., *Inst. Chem. Eng. Symp.*, Ser. 30, p. 136 (1968).

Manuscript received May 24, 2001, and revision received Feb. 12, 2002.